Europe PMC Funders Group
Author Manuscript
Nat Immunol. Author manuscript; available in PMC 2020 September 16.

Published in final edited form as:
Nat Immunol. 2020 April ; 21(4): 388–399. doi:10.1038/s41590-020-0622-8.

A molecular network regulating the pro-inflammatory phenotype of human memory T lymphocytes

Stefan Emming[#1,2], **Niccolò Bianchi**[#1,2], **Sara Polletti**[#3], **Chiara Balestrieri**[3], **Cristina Leoni**[1], **Sara Montagner**[1], **Michele Chirichella**[1], **Nicolas Delaleu**[4], **Gioacchino Natoli**[3,5], **Silvia Monticelli**[1,*]

[1]Institute for Research in Biomedicine (IRB), Università della Svizzera italiana (USI), Via Vincenzo Vela 6, CH-6500, Bellinzona, Switzerland [2]Graduate School for Cellular and Biomedical Sciences; University of Bern, 3012 Bern, Switzerland [3]IEO, European Institute of Oncology IRCCS, Department of Experimental Oncology, Via Adamello 16, 20139 Milano, Italy [4]2C SysBioMed, 6646 Contra, Switzerland, Institute of Oncology Research, Oncology Institute of Southern Switzerland, USI, 6500 Bellinzona, Switzerland and Department of Clinical Medicine, University of Bergen, 5021 Bergen, Norway [5]Humanitas University, Via Rita Levi Montalcini 4, 20090 Pieve Emanuele, Milan, Italy

[#] These authors contributed equally to this work.

Abstract

Understanding the mechanisms that modulate T helper lymphocyte functions is crucial to decipher normal and pathogenic immune responses in humans. To identify molecular determinants influencing the pathogenicity of T cells, we separated *ex vivo*-isolated primary human memory T lymphocytes based on their ability to produce high levels of inflammatory cytokines. We found that the inflammatory, cytokine-producing phenotype of memory T lymphocytes was defined by a specific core gene signature and was mechanistically regulated by the constitutive activation of the NF-κB pathway and by the expression of the transcriptional repressor BHLHE40. BHLHE40 attenuated the expression of anti-inflammatory factors, including miR-146a, a negative regulator of NF-κB activation, and ZC3H12D, an RNase of the Regnase-1 family able to degrade inflammatory transcripts. Our data reveal a molecular network regulating the pro-inflammatory phenotype of human memory T lymphocytes, with the potential to contribute to disease.

Users may view, print, copy, and download text and data-mine the content in such documents, for the purposes of academic research, subject always to the full Conditions of use:http://www.nature.com/authors/editorial_policies/license.html#terms

[*]Corresponding author: silvia.monticelli@irb.usi.ch.

Data availability. All Nanostring, RNA-seq, ChIP-seq and ATAC-seq datasets are available in GEO with accession number GSE122946. Source data are provided for Figure 4e and 5b. Other supporting raw data are available from the corresponding author upon request.

Author Contributions

S.E., N.B., C.L., S. Montagner, and M.C. designed and performed experiments and analyzed data; S.P., C.B. and G.N. performed and analyzed all the sequencing experiments; N.D. analyzed data; S.M. overviewed the project and analyzed data. S.M. and G.N. wrote the manuscript with input from all authors.

Competing interest

The authors declare no competing financial interests.

Europe PMC Funders Author Manuscripts
Europe PMC Funders Author Manuscripts

Europe PMC Funders Author Manuscripts

Europe PMC Funders Author Manuscripts

Keywords

T helper lymphocytes; transcription factors; microRNAs; cytokines; autoimmunity; inflammatory disease

Introduction

Although memory T lymphocytes are catalogued into discrete subsets characterized by the ability to produce specific cytokines, *in vivo* they constitute a continuum ranging from anti-inflammatory to highly pro-inflammatory phenotypes[1]. At population level, T cells are also heterogeneous in terms of their ability to express cytokines, giving rise to stable cytokine-producing and non-producing subpopulations[2]. Understanding mechanisms that play a key role in generating such population diversity and in tipping the balance towards a defined phenotype therefore remains crucial to decipher normal and pathogenic immune responses.

A mechanistic definition of the regulatory circuits underlying the ability of memory T cells to produce pro-inflammatory cytokines will contribute to understand the pathogenesis of immune-mediated diseases. For instance, although myelin-reactive $CD4^+$ T cells are found at similar frequencies in the blood of healthy donors and patients with multiple sclerosis (MS), in MS patients they show a more pro-inflammatory profile[3]. Therefore, it is not the frequency but rather the phenotype of such autoreactive T cells that primarily discriminates between homeostasis and disease. However, the mechanisms underlying the induction of such strongly pro-inflammatory phenotype of T cells are incompletely understood.

GM-CSF (granulocyte-macrophage colony-stimulating factor) is elevated in T cells from patients with MS[4, 5]. GM-CSF expression is critical for the development and maintenance of chronic inflammatory disorders and autoimmune diseases, in which it stimulates innate and adaptive immune responses and amplifies tissue inflammation[4, 6]. It is abundant in the synovium of rheumatoid arthritis patients, whose treatment with antibodies against GM-CSF or its receptor showed clinical efficacy[7, 8]. Conversely, recurrence of disease was observed upon treatment of patients with GM-CSF[9]. Consistently, deletion of the *Csf2* gene, encoding GM-CSF, protected mice from autoimmunity in models of experimental autoimmune encephalomyelitis (EAE), autoimmune myocarditis and collagen-induced arthritis[10, 11, 12, 13].

These observations prompted us to use GM-CSF production as a proxy of the pro-inflammatory potential of primary human memory T lymphocytes. We separated *ex vivo*-isolated human $CD4^+$ T cells based on their capacity to produce GM-CSF and other inflammatory cytokines and we determined the molecular networks controlling inflammatory cytokine expression in these cells. First, we identified a core gene signature associated with a general, cytokine-producing, pro-inflammatory phenotype of human memory T lymphocytes. Among these genes, we found that the high cytokine-producing phenotype was characterized by the preferential expression of the transcriptional repressor BHLHE40 and by increased NF-κB activation. BHLHE40 limited the expression of ZC3H12D, an RNase of the Regnase-1 family able to degrade inflammatory transcripts[14],

Europe PMC Funders Author Manuscripts

Europe PMC Funders Author Manuscripts

and of miR-146a, a negative modulator of NF-κB activation[15], thereby contributing to the regulation of cytokine expression in T lymphocytes.

Results

The gene expression program of GM-CSF-producing human T lymphocytes

We first measured the expression of GM-CSF in naïve (T_N), central memory (T_{CM}) and effector memory (T_{EM}) $CD4^+$ T cells. After stimulation, GM-CSF protein and mRNA expression were highest in T_{EM}, lowest in T_N and intermediate in T_{CM} cells (Fig. 1a,b). Since they expressed the highest levels of GM-CSF, T_{EM} cells were further separated by cytokine-secretion assay in two fractions consisting of GM-CSF-expressing (GM-CSF^+) and non-expressing (GM-CSF^-) cells (Extended Data 1a and Fig. 1c). RNA-sequencing (RNA-seq) was then performed on GM-CSF^+ and GM-CSF^- cells obtained from 9 healthy donors (pooled in three groups) and 678 differentially expressed genes were identified (Fig. 1d and Suppl. Table 1). Principal component analysis (PCA) confirmed that the major differences between samples were attributed to the cell phenotype, with limited donor-to-donor variability (Extended Data 1b). Analysis of the differentially expressed genes confirmed the enrichment of *CSF2* transcripts in the GM-CSF^+ population, together with transcripts from the co-regulated *IL3* gene (Fig. 1d). Genes encoding activation markers such as *CD69*, *IL2RA*, *CD44* and *FASLG* were not differentially expressed, indicating that both the GM-CSF^+ and GM-CSF^- fractions were stimulated to a similar extent. Expression of co-stimulatory molecules such as *CD28* or *ICOS* did not differ between the two subsets, and no components of the TCR complex were differentially expressed.

Several genes linked to a high cytokine-producing, pro-inflammatory phenotype were enriched in the GM-CSF^+ fraction, including *IL22, IFNG* and *TBX21* (Fig. 1d). When considering functional categories, most transcripts encoding for cytokines and chemokines were enriched in the GM-CSF^+ fraction together with the transcripts encoding for the transcription factors (TFs) *RORC*, *TBX21* and *BHLHE40* (Fig. 1e). Genes encoding for T_H1 markers such as *CCR5* and *CXCR3* were detectable at similar levels in both populations (Fig. 1e) and at a protein level GM-CSF was often co-expressed with other subset-defining cytokines such as IL-22, IL-17A and IFN-γ (Extended Data 2a). Overall, the GM-CSF^+ population did not match a unique T cell subset, but it rather represented a pro-inflammatory population characterized by high cytokine-production. Concordant with this notion, genes encoding for chemokine receptors that are commonly used to define rare human T cell subsets such as *CCR6* (T_H17) or *CCR10* (T_H22) were undetectable. In agreement with the requirement of IL-23 for the acquisition of pathogenicity by T_H cells and for their ability to express GM-CSF[10, 16], the *IL23R* gene was higher expressed in GM-CSF^+ than in GM-CSF^- cells (Extended Data 2b).

While GM-CSF^+ cells exhibited a high-cytokine producing phenotype, the GM-CSF^- fraction was enriched for genes linked to the negative regulation of T cell activation, including *IKZF2*, *FOXP3, TIGIT* and *CTLA4* (Fig. 1e). However, other genes associated with a regulatory or exhausted phenotype were not differentially expressed (e.g. *PDCD1*, *HAVCR2*, *LAG3*), not expressed at detectable levels (*UTS2, CECAM4*, *NT5A*, *CD244*) or expressed at higher levels in the GM-CSF^+ subset (*NKG7, ENC1*) (Fig. 1e and Suppl. Table

Europe PMC Funders Author Manuscripts

Europe PMC Funders Author Manuscripts

1). This suggests that GM-CSF^{-} cells may represent a subpopulation of T_{EM} subjected to active repression by the preferential expression of inhibitory proteins. Indeed, the expression of some of these inhibitory receptors can be observed on both regulatory T (T_{reg}) cells and activated conventional T cells (*e.g.* PD-1, LAG-3, TIGIT), although expression on T_{reg} cells is usually higher[17]. Consistent with this possibility, FOXP3 expression was detectable in T_{reg} cells but not in GM-CSF^{-} cells (Extended Data 2c). Additional genes restraining inflammation and autoimmunity in mice such as *BTN2A2* (butyrophilin-2A2, a member of the B7 family of co-stimulatory molecules) were expressed at higher levels in GM-CSF^{-} cells.

We next identified the biological processes associated with the genes differentially expressed in GM-CSF^{+} *vs.* GM-CSF^{-} T_{EM} cells (Fig. 1f and Extended Data 3). Out of 25,127 gene sets analyzed, 119 yielded significant enrichment in GM-CSF^{+} cells (q <0.01, nom. p-value of < 0.005), pointing to five major biological themes (Fig. 1f and Extended Data 3). Pathways pertaining to inflammation, cytokine production, chemotaxis and cell migration were significantly enriched in GM-CSF^{+} cells. A cluster including pathways related to transcription and translation suggests increased activity and protein synthesis of GM-CSF^{+}, cytokine-secreting cells. In the remaining cluster, response to vitamin D, containing both the vitamin D receptor gene (*VDR*) and the 25-Hydroxyvitamin D3 1-alpha-hydroxylase-encoding gene (*CYP27B1*), was the most significantly enriched gene set (q = 0.0016). Notably, vitamin D deficiency is associated with the risk of developing autoimmune disorders[18, 19], suggesting that T cells with high inflammatory cytokine-expressing potential have also intrinsic mechanisms to dampen their activity. Overall, these data suggest that the GM-CSF^{-} T cells represent a population of T_{EM} cells subjected to active repression mechanisms that restrain their inappropriate activation.

BHLHE40 expression correlates with a pro-inflammatory phenotype

We used qRT-PCR to confirm the differential expression of several TFs and other relevant genes identified by RNA-seq in samples obtained from additional donors (Fig. 2a). *RORC*, *BHLHE40* and *TBX21* were the most differentially expressed TF genes in the GM-CSF^{+} population, while *FOXP3* and to a lesser extent *AHR* were enriched in the GM-CSF^{-} fraction. We then determined whether the identified signature genes were more generally associated with a pro-inflammatory cytokine-producing T cell phenotype and not with features related specifically to T_{EM} cells. We therefore repeated the expression profiling of ~570 immune-related genes using GM-CSF^{+} and GM-CSF^{-} T_{CM} cells from six independent donors (pooled in 2 groups), analyzed by Nanostring digital counting (Suppl. Table 2). We found a high correlation (R^2=0.7793, P<0.0001) between T_{EM} and T_{CM} cells in terms of genes that were differentially expressed in the GM-CSF^{+} and GM-CSF^{-} subpopulations (Extended Data 4a). Genes encoding for activation markers and co-stimulatory molecules (e.g. *IL2RA, CD28, CD40L*) were not differentially expressed. The *IL2* transcript, which is highly expressed by this memory subset, was also not differentially expressed. As with T_{EM} cells, many cytokine genes, including *IL3*, *IL22*, *IL17A* and *IFNG* were preferentially expressed by GM-CSF^{+} cells, while *TIGIT* and *CTLA4* were associated with the GM-CSF^{-} fraction. However, some differentially expressed genes were specific of the T_{EM} phenotype rather than representing general features of cytokine-secreting or non-secreting cells. This

Europe PMC Funders Author Manuscripts

Europe PMC Funders Author Manuscripts

latter category included *IL10* and *FOXP3* (Fig. 2b). Importantly, the *BHLHE40* gene was preferentially expressed also by T_{CM} GM-CSF$^+$ cells (Fig. 2c), suggesting a possible function for this transcriptional repressor in regulating the inflammatory cytokine-producing phenotype of T cells. Concordant with this possibility, we found that *BHLHE40* was strongly expressed by T_H1 and T_H17 cells, and especially by the highly pro-inflammatory $T_H1/17$ (also known as T_H1^*) lymphocyte subset (Fig. 2d)[20]. *BHLHE40* was also expressed at significantly higher levels in T_{EM} cells than T_{CM} cells, correlating with higher effector cytokine production (Extended Data 4b).

We further narrowed down our pro-inflammatory T cell gene signature by excluding genes that might be specifically associated to GM-CSF secretion. Gene expression analyses were repeated using T_{EM} cells separated based on their ability to secrete IL-22. We selected this cytokine because similarly to GM-CSF, and differently for instance from IL-17, it is easily detectable in memory T cells freshly separated from peripheral blood, and it is not expressed at levels that are too high (like IFN-γ) that would thus easily generate false positive results. IL-22-producing cells are contained primarily in the T_{EM} subset (Fig. 2e) and they are not a subset of the more frequent GM-CSF-producing ones, since T_{EM} cells that were either double- (GM-CSF$^+$ and IL-22$^+$) or single-producers (either GM-CSF$^+$ or IL-22$^+$) were observed (Extended Data 2a). Despite the low fraction of IL-22-producing cells, we retrieved similar percentages by secretion assay and intracellular cytokine staining (Fig. 2f). At mRNA level, the IL-22$^+$ population expressed the *IL22* transcript >120-times higher compared to the IL-22$^-$ population (Fig. 2g). By analyzing the expression of selected genes in IL-22$^+$ and IL-22$^-$ cells, we retrieved many genes already identified as associated with the GM-CSF$^+$ phenotype, indicating that these genes can be considered as a general signature defining cytokine-producing memory T cells. This included the core signature genes *IL22*, *CSF2*, *IL17A* and *IL23R*. Most importantly, *BHLHE40* was the predominant differentially expressed TF gene, followed by *RORC* and *TBX21* (Fig. 2g). Overall, these data show a strong correlation between *BHLHE40* expression and high inflammatory potential of human T lymphocytes.

Identification of BHLHE40 as a regulator of gene expression in human T lymphocytes

To identify TFs regulating the genes distinctive of the GM-CSF$^+$ and the GM-CSF$^-$ populations, we identified over- or under-represented TF consensus DNA-binding motifs in the regions surrounding the transcription start sites (TSSs, from -450 bp to +50 bp) of the differentially expressed genes (Suppl. Table 3). NF-κB binding sites were enriched upstream of the genes more highly expressed in the GM-CSF$^+$ population (Fig. 3a). Consistent with a repressive activity of BHLHE40, its transcript was highly expressed by GM-CSF$^+$ and IL-22$^+$ cells (Fig. 2), but its binding sites were instead enriched upstream of genes preferentially expressed in the GM-CSF$^-$ population. These data suggest that BHLHE40 expression in GM-CSF$^+$ T cells may contribute to the repression of genes preferentially expressed in GM-CSF$^-$ cells.

To obtain a broader view of the genomic regulatory landscape of GM-CSF$^+$ and GM-CSF$^-$ T cells, we performed ATAC-seq experiments in primary T_{EM} cells separated by GM-CSF secretion assay. We detected >100,000 peaks per sample, with 1,438 regions being specific

Europe PMC Funders Author Manuscripts

Europe PMC Funders Author Manuscripts

for GM-CSF^{-}cells and 1,318 for GM-CSF^{+} cells (FDR<0.01 and $\log_2$FC>1) (Fig. 3b). First, we confirmed the correlation between ATAC-seq peaks and differential expression of adjacent gene(s). For instance, the locus containing the *CSF2* and *IL3* genes showed differential ATAC-seq peaks that were specifically detected in the GM-CSF^{+} cells (Fig. 3c); the *FCRL3* locus was instead selectively accessible in GM-CSF^{-} cells (Fig. 3c and Extended Data 4c).

The analysis of the TF motifs underlying the ATAC-seq peaks confirmed the enrichment of NF-κB motifs in the comparison of GM-CSF^{+} *vs.* GM-CSF^{-} specific peaks (Fig. 3d and Suppl. Table 4). GM-CSF^{+} peaks were also significantly enriched for BHLHE40 sites, suggesting that BHLHE40 may bind and induce repression of genomic regulatory elements in GM-CSF^{+} T cell. However, the magnitude of the over-representation was relatively lower, indicating that BHLHE40 sites selectively accessible in GM-CSF^{+} T cells were in limited number. ATAC-seq peaks specific of GM-CSF^{-} T cells showed instead a strong over-representation of cognate motifs for Interferon Regulatory Factor (IRF) family members (Fig. 3d), including those in the proximity of some negative regulators of T cell activation such as *TIGIT* and *FCRL3*. Specifically, 887/1,438 (61.6%) ATAC-seq regions selective for GM-CSF^{-} T cells contained high-affinity IRF sites (Suppl. Table 5). To identify TFs modulating the inflammatory phenotype of memory T lymphocytes, we integrated the motif analysis on ATAC-seq data with expression data for TF families matching over/under represented TF motifs. A few TF motifs significantly enriched in the GM-CSF^{+} or GM-CSF^{-} ATAC data, matched TFs differentially expressed in the same population (Suppl. Table 4). Among these, we found that increased expression of *BHLHE40*, *TBX21* and *VDR* in the GM-CSF^{+} cells was associated with increased accessibility of their binding sites, pointing towards a relevant role for these factors in favoring (*TBX21*) or restraining (*VDR*) the inflammatory phenotype of these cells (Fig. 3e). The GM-CSF^{-} cells showed instead higher expression of *FOXP3* and *IRF3*, which were associated with increased accessibility of their binding sites specifically in these cells.

BHLHE40 (SHARP-2, STRA13, DEC1) is a basic helix-loop-helix (bHLH) TF reported to regulate immune cell functions. In the mouse, *Bhlhe40* expression was associated with a pathogenic T cell signature and it was shown to identify the cytokine-producing fraction of autoreactive T cells[21]. *Bhlhe40* deletion increased resistance to EAE induction and diminished expression of GM-CSF, IFN-γ, IL-2 but also IL-4, while expression of IL-10 was increased[21, 22, 23, 24, 25, 26]. However, the initial description of the *Bhlhe40*$^{-/-}$ phenotype revealed development of autoimmune disease in aging animals, with the accumulation of spontaneously activated lymphocytes[22], linked to reduced T_{reg} cell numbers[27].

To assess the functional role of BHLHE40 in primary human T lymphocytes, we performed CRISPR-Cas9-mediated deletion of *BHLHE40*. After optimizing screening methods[28] (Extended Data 5), we transfected primary memory human T lymphocytes with Cas9 ribonucleoparticles against *BHLHE40*, and performed single-cell cloning[29, 30]. We next measured GM-CSF expression by intracellular staining, comparing control clones to clones that showed deletions in the *BHLHE40* locus between exon 1/2 and exon 5 (locations of the sgRNAs), as determined by PCR (hereafter, 'BHLHE40-KO' clones). In both BHLHE40-KO and control clones, GM-CSF expression became detectable in most cells due to the

Europe PMC Funders Author Manuscripts

Europe PMC Funders Author Manuscripts

extensive proliferation and high IL-2 concentration required for cloning[5]. Despite this limitation and the high gene expression variability of human T cell clones, we measured a significant reduction in GM-CSF expression in BHLHE40-KO clones compared to controls (Fig. 3f). A significant reduction was also observed for other inflammatory cytokines (Extended Data 6). Reduced GM-CSF protein and mRNA expression was observed in additional clones generated with a smaller *BHLHE40* deletion (Fig. 3g). Consistent with these results, lentivirus (LV)-mediated expression of BHLHE40 in primary lymphocytes (Fig. 4a) increased GM-CSF- and IL-17A expression (Fig. 4b). Analysis of cytokine mRNA expression by Nanostring profiling in primary memory T lymphocytes transduced to express BHLHE40, revealed a shift towards an inflammatory T_H17 GM-CSF$^+$ phenotype (Fig. 4c and Suppl. Table 6). *CSF2* mRNA expression was also observed in Jurkat T cells stably expressing BHLHE40 (Fig. 4d). BHLHE40 can influence gene transcription either through direct DNA binding or by competing with other E-box-binding factors[31, 32]. We therefore assessed whether BHLHE40 impacted expression of a luciferase reporter gene with four BHLHE40 consensus binding sites upstream of a minimal promoter. BHLHE40 repressed reporter gene expression (Fig. 4e), while a C-terminal truncated version (BHLHE40 1-297aa) retaining DNA-binding activity and acting in a dominant-negative manner [31, 33, 34], was devoid of effects. These data confirm a role for BHLHE40 in regulating the pro-inflammatory phenotype of human memory T lymphocytes, most likely acting as a transcription repressor.

Basal NF-κB activation in GM-CSF$^+$ T lymphocytes

The NF-κB motif was over-represented in the promoter regions of genes differentially expressed in the GM-CSF$^+$ population. The transcripts encoding NF-κB family members were instead expressed at comparable levels in both populations, which is consistent with post-transcriptional NF-κB activation. We therefore measured NF-κB activation in GM-CSF$^+$ and GM-CSF$^-$ T cells using as readouts the phosphorylation of p65/RELA at Ser529 and of IκBα at Ser32/36. Phosphorylation of p65 was shown to be significantly increased in lymphocytes from MS patients (which also showed increased GM-CSF production)[35]. We found that phosphorylation of NF-κB p65 and IκBα were significantly higher in GM-CSF$^+$ compared to GM-CSF$^-$ lymphocytes (Fig. 5a). A significant difference in NF-κB p65 phosphorylation was confirmed by immunoblot (Fig. 5b). Overall, the combination of enhanced BHLHE40 expression and increased NF-κB activation may regulate the pro-inflammatory phenotype of human T lymphocytes.

BHLHE40 expression and NF-κB activation converge on the regulation of miR-146a expression

To understand the molecular mechanisms that regulate the pro-inflammatory T cell phenotype with elevated cytokine production, we analyzed global miRNA expression in GM-CSF$^+$ and GM-CSF$^-$ T_{EM} cells by Nanostring profiling. We found very little differences in miRNA expression when subdividing T_{EM} cells based on their ability to secrete GM-CSF, with only two miRNAs, miR-181a and miR-146a, being enriched in the GM-CSF$^-$ population (Fig. 6a and Suppl. Table 7). Increased miR-146a and miR-181a expression was also observed in IL-22$^-$ T_{EM} cells (Fig. 6b). The differential expression of these miRNAs in the cytokine-negative fraction suggested that they might contribute to

Europe PMC Funders Author Manuscripts

Europe PMC Funders Author Manuscripts

maintain this population in a repressed, less inflammatory state. We focused on miR-146a, an established negative regulator of NF-κB activation[15]. To determine whether miR-146a influences NF-κB activation in primary human T lymphocytes, we transfected freshly isolated memory T cells with either a miR-146a mimic or a control oligonucleotide. After two days, cells were stimulated with PMA and ionomycin for 5 minutes, followed by intracellular staining for the phosphorylated forms of NF-κB p65 and IκBα. The miR-146a mimic significantly reduced NF-κB p65 phosphorylation, and a similar trend was also observed for IκBα (Fig. 6c). Concordant with these results, transduction of primary human T lymphocytes with a miRNA sponge to sequester miR-146a and reduce its activity, led to increased p65 phosphorylation (Extended Data 7a-b).

Since BHLHE40 was differentially expressed between cytokine-producing and non-producing cells, and it was also involved in the regulation of cytokine expression, we asked whether it could contribute to the observed differential expression of miR-146a. We stably expressed BHLHE40 in Jurkat T cells by lentiviral transduction, followed by stimulation to induce miR-146a expression[36]. BHLHE40 expression significantly reduced miR-146a induction compared to the control (Fig. 6d). Similar results were obtained in primary T lymphocytes (Fig. 6e). This was not the case for miR-181a, whose regulation in this context remains to be understood (Fig. 6e and Extended Data 7c). Consistent with these results, phosphorylation of NF-κB p65 in primary T cells overexpressing BHLHE40 was significantly, albeit modestly increased (Fig. 6f). Overall, miR-146a regulates NF-κB activation in primary human T lymphocytes, and its increased expression in cytokine-negative cells is likely to maintain NF-κB p65 phosphorylation at lower basal levels compared to cytokine-positive cells.

BHLHE40 binding sites reveal high genomic specificity

We set out to identify genes bound by BHLHE40. Since commercially available antibodies did not generate robust results in human T cells, we stably transduced Jurkat T cells to express Flag-tagged BHLHE40 and we carried out ChIP-seq using an anti-flag antibody (Fig. 7a). Many of the 2,356 ChIP-seq peaks were at promoter regions (Fig. 7b), highlighting the possibility of direct transcriptional regulation of the associated genes. A motif analysis recovered with the highest significance the E-box, namely the consensus sequence for bHLH (including Hairy-related) TFs (Fig. 7c); moreover, the most enriched E-box motif was the variant specifically recognized by BHLHE40 (Extended Data 7d and Suppl. Table 8). The high specificity of BHLHE40 recruitment to this variant motif appears to be linked to the presence of a highly-conserved K (T or G) base 5′ of the CACGTG core sequence and an M (C or A) base 3′ of it.

The functional analysis of the genes associated with the genomic regions bound by BHLHE40 revealed categories relevant to the biology of this factor, including those related to T cell differentiation and circadian clock (Fig. 7d and Suppl. Table 8), with the latter category including the clock gene *PER1*. Concordant with previous work[24, 25], we could not detect any binding of BHLHE40 in the proximity of most cytokine genes, including *CSF2*. A direct regulation of cytokine expression appears therefore unlikely. Similar to the *CSF2* gene, the effect of BHLHE40 on miR-146a expression appears to be indirect, since no

Europe PMC Funders Author Manuscripts

Europe PMC Funders Author Manuscripts

significant binding could be detected in the proximity of the miR-146a locus. Other significant functional categories included “regulation of mRNA stability” and “single-stranded RNA binding”. This result drew our attention to one of the genes containing a prominent BHLHE40 peak, namely that encoding for ZC3H12D, an RNase belonging to the same family of Regnase-1 (ZC3H12A), a negative regulator of inflammation which acts through the degradation of inflammatory gene transcripts[37].

To investigate the relevance of BHLHE40 binding at *ZC3H12D* and other loci, we intersected the list of differentially expressed genes in GM-CSF$^+$ *vs.* GM-CSF$^-$ cells with ChIP-seq data (Suppl. Table 8). 118 genes downregulated in the GM-CSF$^+$ cells were bound by BHLHE40 (including *ZC3H12D*), suggesting direct repression. Conversely, only 51 upregulated genes were also bound by BHLHE40. By comparing our ChIP-seq data with published Bhlhe40 ChIP-seq data[25] from mouse Th1 cells, we found that 573 genes were retrieved in both datasets (Fig. 7e). Regions identified as bound by BHLHE40 in both datasets included those associated with *PER1*, *BHLHE40* and most importantly *ZC3H12D*, suggesting conservation of regulatory networks.

The overall pattern of accessibility at regions bound by BHLHE40 was not dramatically different in GM-CSF$^+$ *vs.* GM-CSF$^-$ cells, as determined by ATAC-seq in primary human T lymphocytes. Specifically, only a small number of differentially accessible regions matched BHLHE40 ChIP-seq peak within a window of 150bp, while 1,880 BHLHE40 bound peaks were accessible in both GM-CSF$^+$ and GM-CSF$^-$ cells. Interestingly, an ATAC-seq peak corresponding to BHLHE40 binding was observed in the *ZC3H12D* promoter region (Fig. 7f). These observations suggest that functional BHLHE40 sites are contained within regions that are accessible in both GM-CSF$^+$ and GM-CSF$^-$ cells and can be thus considered as poised negative regulatory elements whose final output ultimately depends on BHLHE40 expression and binding.

ZC3H12D is negatively regulated by BHLHE40

Next, we investigated the regulation of *ZC3H12D* by BHLHE40. Both ZC3H12A and ZC3H12D induce the degradation and turnover of mRNAs involved in inflammation[14, 38]. Deficiency of *ZC3H12D* in mice led to increased stability of cytokine mRNAs, increased levels of IL-17A and severe paralysis in EAE models, highlighting a role in modulating the pro-inflammatory phenotype of T lymphocytes[39]. Consistent with a negative regulation by BHLHE40, *ZC3H12D* (but not *ZC3H12A*) was differentially expressed in GM-CSF$^-$ cells (Fig. 8a); moreover, Jurkat T cells stably expressing BHLHE40 showed reduced expression of *ZC3H12D* but not of *ZC3H12A* (Fig. 8b). We next determined whether BHLHE40 had a direct effect on *ZC3H12D* transcription by luciferase reporter assays using a region of the *ZC3H12D* promoter (from -285 to +349 relative to the TSS) corresponding to both the ChIP-seq and the ATAC-seq peaks shown in Fig. 7f. BHLHE40 expression reduced the luciferase activity of plasmids containing the wild-type *ZC3H12D* promoter, but not that of a promoter containing mutated BHLHE40 binding sites (Fig. 8c). Luciferase expression from the mutated plasmid was also significantly higher than that from the wild-type construct in cells not over-expressing BHLHE40, possibly because of the inability of endogenous BHLHE40 to bind and repress.

Europe PMC Funders Author Manuscripts

Europe PMC Funders Author Manuscripts

Finally, using the knock-out clones described above, we found that *BHLHE40* gene loss increased *ZC3H12D* expression (Fig. 8d). These data therefore suggest that BHLHE40 modulates the pro-inflammatory phenotype of primary human memory T lymphocytes, at least in part through the direct repression of anti-inflammatory genes such as *ZC3H12D*.

ZC3H12D is a negative regulator of cytokine expression

To further investigate to what extent ZC3H12D acts as an anti-inflammatory regulator, we first performed luciferase reporter assays to determine the impact of ZC3H12D on the 3′UTR of inflammatory cytokines mRNAs, cloned downstream a luciferase reporter gene. Expression of ZC3H12D, but not of a mutant version lacking RNase activity (D95N)[14] significantly reduced luciferase expression in constructs containing the *TNF* and *IL22* 3′UTR (Fig. 8e). Next, we used CRISPR-Cas9 and single-cell cloning to delete *ZC3H12D* in primary human memory $CD4^+$ T lymphocytes. We selected clones (from two independent donors) that showed a high percentage of indels at mismatch cleavage assay (Extended Data 5), and we measured cytokine mRNA expression. The expression of *TNF* and *IL22* was strongly and significantly increased in absence of ZC3H12D (Fig. 8f). The expression of *CSF2* was also increased, although cultured T cell clones acquire spontaneously the ability to produce very high amounts of this cytokine (Fig. 3f-g), making it more difficult to detect further changes.

Altogether, our data revealed that the highly inflammatory, cytokine-producing phenotype of primary human T lymphocytes is mechanistically regulated by a module comprising miR-146a, the RNase ZC3H12D and the TFs NF-κB and BHLHE40 (Extended Data 8).

Discussion

Here, we identified a regulatory module composed of the TFs BHLHE40 and NF-κB, the miRNA miR-146a and the RNAse ZC3H12D that contributes to balance the pro-inflammatory potential of human memory T lymphocytes.

In our experiments, the transcripts encoding BHLHE40, RORγt and T-BET were systematically and reproducibly part of a T lymphocyte pro-inflammatory signature. These factors are involved in autoimmune diseases, in some cases partially independently of the cytokines they primarily regulate. For example, loss of T-BET, the master TF of IFN-γ-producing T_H1 cells, was shown to render mice more resistant to EAE, although loss of IFN-γ or its receptor left mice susceptible to autoimmunity[40, 41]. In general, lineage-determining TFs are often co-expressed either stably or transiently and work in a collaborative fashion, thus leading to a variety of outcomes and distinct T cell phenotypes[42]. For instance, murine invariant natural killer (iNKT) cells deficient for *Bhlhe40* were significantly impaired in their ability to produce IFN-γ, but no direct effect of this TF was observed on the *Ifng* promoter. In this context, Bhlhe40 acted instead as a cofactor, physically interacting with and enhancing T-bet activity[43]. Interestingly, a subset of T_H1-like T cells defined by BHLHE40 expression was recently found expanded in samples of colorectal cancer from patients with microsatellite-instability, who display favorable responses to treatment with immune checkpoint inhibitors[44]. These data underline how this TF may be indeed involved

Europe PMC Funders Author Manuscripts

Europe PMC Funders Author Manuscripts

in ‘tipping the balance’ of T cell responses, from beneficial for cancer immune therapy to potentially pathogenic in autoimmunity.

Adding to the complexity in fully understanding the mechanisms underpinning TF functionality, several TFs pivotal for immune functions possess both activating and repressive functions on gene expression in T lymphocytes, with different mechanisms of action. For example, PU.1 regulates gene expression early during T cell development not only by recruiting partner TFs to its own binding site, but also by depleting them from distant binding sites that they would otherwise occupy in the absence of PU.1[45]. Similarly, T-BET employs different strategies to repress transcription of genes belonging to lineage decisions different to that of T_H1 cells[46]. While we still do not fully understand how BHLHE40 exerts its transcriptional effects, we can envision the possible cooperation as well as competition with other partners, depending on the relative concentration of each factor and binding affinity. These effects may also be direct as well as indirect, depending on the DNA binding site and its context. For example, even though Bhlhe40 was shown to regulate IL-10 expression in response to infection, and even to bind to the *Il10* locus in the mouse, it remains unclear whether Bhlhe40 exerts its transcriptional effects on this locus directly[25, 26]. Indeed, Bhlhe40 binds the mouse *Il10* locus in a likely regulatory region downstream of the 3′-end of the gene, and not at its promoter[25]. Similar secondary effects on gene expression may also include the control of miR-146a expression.

Given the complexity in fully understanding the mechanism of action of BHLHE40, it is likely that this TF may belong to a functional category of regulators of transcription that requires accessible chromatin, a specific DNA sequence, and also interaction with additional cofactors that drive selectivity and final functional outcome. Overall, our work identified a molecular module involved in regulating the highly cytokine-producing, pro-inflammatory and potentially pathogenic phenotype of primary human $CD4^+$ memory T lymphocytes, pointing towards specific TFs and miRNAs that may be dysregulated during disease.

Methods

Primary human T cell isolation and culture

Blood from healthy donors was obtained from the Swiss Blood Donation Center of Basel and Lugano (Switzerland), with informed consent from the Swiss Red Cross and authorization number CE 3428 from the Comitato Etico Canton Ticino. $CD4^+$ T cells were separated by gradient centrifugation (Ficoll-Paque Plus; GE Healthcare), followed by positive selection using magnetic microbeads (Miltenyi Biotec). T cell subsets were then sorted using a FACSaria (BD Bioscience) based on the expression of the following surface markers: naïve T cells: $CD4^+CD25^-CD45RA^+CCR7^+$; total memory T cells: $CD4^+CD25^-CD45RA^-CCR7^{+/-}$; T_{CM}: $CD4^+CD25^-CD45RA^-CCR7^+$; T_{EM}: $CD4^+CD25^-CD45RA^-CCR7^-$. Other T cell subsets were separated as follows: T_H1: $CD4^+CD25^-CD45RA^-CXCR3^+CCR4^-$ $CCR6^-$; T_H2: $CD4^+CD25^-CD45RA^-CXCR3^-CCR4+CCR6^-$; T_H17: $CD4^+CD25^-CD45RA^-CXCR3^-CCR4^+CCR6^+$; T_H1*: $CD4^+CD25^-CD45RA^-CXCR3^+CCR4^+CCR6^+$; T_{reg}: $CD4^+CD25^{hi}CD127^{lo}$. When needed, sorted T cell subsets were cultured in RPMI-1640 medium supplemented with 5% human serum, 1% non-essential amino acids, 1%, sodium pyruvate, 1% glutamine, penicillin, streptomycin and 50

Europe PMC Funders Author Manuscripts

Europe PMC Funders Author Manuscripts

μM β-mercaptoethanol (complete medium). T lymphocytes were stimulated in NUNC™ 96-well plates (Thermo Fisher) using plate-bound anti-CD3 (clone TR66, recombinant, made in house) and anti-CD28 (1 μg/ml). In cases of extended cultures, recombinant IL-2 (50 U/ml) was added starting from day 5.

Generation and culture of T cell knock-out clones

Oligonucleotides corresponding to crRNAs and tracrRNAs (Dharmacon, IDT) were mixed at a final concentration of 80 μM in 10 μl of Nuclease Free Duplex buffer (Dharmacon, IDT), followed by annealing by boiling and cool-down. The protein-RNA complex was prepared immediately before transfection by mixing 7.5 μg of recombinant TrueCut Cas9 Protein v2 (Thermofisher) with 1.5 μl of the crRNA/tracrRNA duplex mix in a total volume of 3 μl followed by incubation for 20 min at ~21°C. Alt-R Electroporation enhancer (Dharmacon, IDT) was added at a final concentration of 1.7 μM. Transfection was performed with the 10 μl Neon Transfection System kit; ~8×10^5 T cells were resuspended in Neon electroporation Buffer R or Buffer T, respectively, and added to the electroporation solution. Cells were then electroporated with 1 pulse, 2200V, width 20ms. After transfection, individual Jurkat cells were cloned by limiting dilution into 384-well plates in RPMI-1640 medium supplemented with 20% FBS, 1% non-essential amino acids, 1%, sodium pyruvate, 1% glutamine, penicillin, streptomycin and 50 μM β-mercaptoethanol. Individual clones were picked and further expanded. Primary T cells were seeded in 384-well plates at 0.5-0.8 cells per well in complete medium in the presence of recombinant IL-2 (500 U/ml), 1 μg/ml of phytohaemagglutinin (PHA) and 2.5×10^4 irradiated (45 Gy) allogeneic feeder cells (peripheral blood mononuclear cells) as previously described[30]. After 2 weeks, individual clones were transferred into round-bottom 96-well plates and further expanded.

Analysis of CRISPR/Cas9 deletions in T cell clones

Genomic DNA (gDNA) from individual clones (3-8 × 10^4 cells) was isolated using the QIAamp DNA Micro Kit (Qiagen). To screen for the presence of deletions/ mutations, a T7 endonuclease cleavage assay was used[28]. PCR primers were designed to amplify a ~1000 bp region surrounding the area targeted by the sgRNAs (“Long PCR”, Extended Data 5). The PCR amplification was performed using the high fidelity KOD Hot Start DNA polymerase (Novagen). 8.5 μl of each PCR product were denatured and re-annealed, followed by addition of 5 units of T7 endonuclease (New England Biolabs). As an independent confirmation of the presence of deletions, we used primers complementary to the deleted region, therefore incapable of generating any PCR product in deleted clones (“Short-PCR”, Extended Data 5).

Secretion assay

Cytokine secretion assays (Miltenyi Biotec) were performed according to the manufacturer’s protocol. Freshly separated cells were stimulated in complete media with PMA (200 nM) and ionomycin (1 μg/ml) for 3h before labelling with the assay’s reagents and sorting.

Europe PMC Funders Author Manuscripts

Europe PMC Funders Author Manuscripts

Intracellular staining

Cells were stimulated for 5h with PMA (200 nM) and ionomycin (1 μg/ml). For the last 2.5h of stimulation, brefeldin A (10 μg/ml) was added to the cells. Cells were fixed with paraformaldehyde (PFA, 4%) and permeabilized with 0.5% BSA and saponine. The antibodies used are listed in Suppl. Table 9. For NF-κB p65 phosphorylation, cells were stimulated for 5-30 min with PMA and ionomycin, fixed with PFA and permeabilized with methanol. For intracellular FOXP3 staining, a FOXP3 Transcription Factor Staining Buffer Set (BD Bioscience) was used. All samples were acquired on a Fortessa flow cytometer (BD Bioscience) and data was analyzed with FlowJo Software.

RNA sequencing

T_{EM} cells obtained from nine independent female donors were separated in GM-CSF^{+} and GM-CSF^{-} fractions by cytokine secretion assay and immediately lysed in TRI reagent (MRC). The samples were divided into three pools of three donors each and RNA extraction was performed using the Direct-Zol RNA mini Prep kit (Zymo Research). mRNA-Seq library preparation from 400 ng of total RNA (RIN >8) was performed with the TruSeq RNA Sample Prep kit v2 (Illumina) according to the manufacturer's instructions, and single-end sequenced on an Illumina HiSeq2000 platform.

Chromatin immunoprecipitation and sequencing (ChIP-seq)

Jurkat T cells (60×10^{6} cells) stably transduced with a flagged version of BHLHE40 or control vector were fixed with 1% formaldehyde. Cells were lysed with RIPA buffer and, after chromatin shearing by sonication, incubated overnight at 4°C with 100 μl of protein G Dynabeads (Invitrogen) previously coupled with 10 μg of anti-Flag M2 antibody (Sigma). After immunoprecipitation, beads were recovered using a magnet and washed as previously described[47]. DNA was eluted, cross-links reverted overnight at 65°C and purified with QiaQuick columns (Qiagen). 3 ng of ChIP-DNA (quantified with the QuantiFluor dsDNA System from Promega) were used to generate ChIP-Seq libraries as described[47]. The amplified DNA was quality checked on a Tapestation system (Agilent) and single-end sequenced on an Illumina NextSeq500 platform.

ATAC-seq

Freshly sorted primary T_{EM} cells from three independent donors were separated into GM-CSF^{+} and GM-CSF^{-} fractions by cytokine secretion assay. Two different protocols of cells lysis were used, which provided similar results and were therefore treated as technical replicates. Briefly, 5×10^{4} GM-CSF^{+} and GM-CSF^{-} cells from each donor were pelleted by centrifugation and resuspended in 50 μl of either Lysis Buffer 1 (10mM Tris-HCl pH 7.4, 10mM $MgCl_2$, 0.1% Igepal CA-630) or Lysis Buffer 2 (10mM Tris-HCl pH 7.4, 3mM $MgCl_2$, 10mM NaCl, 0.1% Igepal CA-630). After incubation on ice for 3 min, nuclei were pelleted by centrifugation for 20 min at 500g, 4ºC, and resuspended in 50 μl of reaction buffer containing 1 μl of Tn5 transposase (made in house), 10 μl of 5× transposase buffer (50mM Tris-HCl, pH 8.4 and 25mM $MgCl_2$), and 39 μl of milliQ water. The reaction was incubated at 37ºC for 60 min, followed by the addition of 10 μl of clean-up buffer (900mM NaCl, 300mM EDTA), 2μl of 10% SDS, 6μl of milliQ water and 2 μl of Proteinase K (20 μg/

Europe PMC Funders Author Manuscripts

Europe PMC Funders Author Manuscripts

μl) (Thermofisher) and incubation for 30 min at 40 ºC. Tagmented DNA was isolated using 2× SPRI beads and amplified by PCR. Fragments smaller than 600 bp were isolated by negative size selection (using 0.65× SPRI beads) and then purified with 1.8× SPRI beads. Libraries were single-end sequenced on an Illumina NextSeq500 platform.

Bioinformatic analysis

i) RNA-seq data analysis—RNA-seq analysis was performed as previously described[48], with minor changes. After quality filtering according to the Illumina pipeline, 50 bp single-end reads were aligned to the human genome (build GRCh38/hg38) using TopHat2 (version 2.1.0) with the option "*--b2-very-sensitive*". Only uniquely mapped reads were retained. At the gene level, expression counts were estimated using HTSeq (version 0.6.1), summarized across all exons as annotated in the GENCODE v25, with option "*union*" and *"no strand-specific assay"*. Both coding and long noncoding RNA genes with a minimum of 1 read count in at least three samples were retained for downstream analyses. Differential expression analysis was performed using the EdgeR R-package (version 3.2.2) with Trimmed Mean of M (TMM) normalization, generalized linear model and likelihood ratio tests. Analyses were performed for each cell type separately and Differential Expressed Genes (DEGs) were identified in pairwise comparisons. Then, Transcript Per Million (TPM) values were used as expression unit. For each differential analysis DEGs were defined on the basis of the following parameters: absolute $\log_2$ fold-change (FC) ≥ 1, false discovery rate (FDR) < 0.001.

ii) ChIP-seq and ATAC-seq data analysis—Raw reads for each ChIP-seq and ATAC-seq dataset were processed using Trimmomatic (version 0.38)[49] to trim off adapter sequences incorporated in the read and to remove low quality bases, using the following parameters "*TRAILING:3 LEADING:3 ILLUMINACLIP:adapters.fasta:2:30:10; SLIDINGWINDOW:4:20 MINLEN:40*" (for ATAC-seq datasets a *MINLEN* = 36 was used). A single ATAC-seq dataset for each condition was obtained by merging four replicates. Then, the resulting reads were mapped to the to human genome build GRCh38/hg38 using Bowtie2 v2.2.6 with the "*--very-sensitive*" preset of parameters. Reads that did not align to the nuclear genome or aligned to the mitochondrial genome were removed and duplicate reads were marked and removed using SAMtools. For ATAC-seq, read positions were corrected for transposon insertion offset as described[50]. Peak calling *vs.* the corresponding input genomic DNA was performed using MACS2 (version 2.1.0.20150731)[51] with the *"--nomodel"*, "*--extsize 200*", *"--keep-dup all"* and "*--qvalue 0.05*" flags and arguments (for ATAC-seq a *extsize* = 146 and "*--nolambda*" and no input was used). TF peaks with a fold enrichment (FE) relative to the input < 5 and those blacklisted by the ENCODE consortium analysis of artifactual signals in human cells (https://sites.google.com/site/anshulkundaje/projects/blacklists) were removed using bedtools[52]. To obtain a high-confidence peaks set, only intersections between biological replicates that overlapped by >50% were retained and shown as heatmap (generated using deepTools version 2.5.3)[52].

The union of open chromatin regions was generated by merging peaks sets from each individual condition and a unique summit of reference was obtained by re-running MACS2 with a unique pooled bam file. Then, each region was extended by 73 bp in both directions

Europe PMC Funders Author Manuscripts

Europe PMC Funders Author Manuscripts

from the peak summit to obtain a homogeneous peak width of 146 bp. Finally, differential binding analysis was performed using DiffBind (version 2.6.6)[53] with settings to use DESeq2 method, full library size and without subtraction of control input read counts. Binding events with an FDR cutoff of 1e-02 and an absolute variation ≥ 1 ($\log_2$ scale) were defined as significantly different among experimental conditions.

To classify peaks based on their genomic location and assign them to the nearest Transcription Start Site (TSS), as annotated in the GENCODE v28 of the human genome, we used the *annotatePeaks* script from the HOMER package[54]. Each peak was classified as either TSS-proximal or TSS-distal, depending on its distance (> or < 2.5 kb, respectively) from annotated TSSs.

Peaks lists were subjected to the functional annotation enrichment analysis using Genomic Regions Enrichment of Annotations Tool (GREAT version 3.0.0)[55] using the entire genome as background and default parameters.

iii) Motif analysis—In order to identify statistically over-represented motifs corresponding to known transcription factor binding sites, a collection of 2,314 position-specific weight matrices (PWMs) were obtained as described[56], and a window of 500 bp (-450 and +50 bp relative to TSS) or a window of 300 bp (centered on the summit of ATAC-seq peaks) was used. Significantly over-represented PWMs between two sets were identified using a modified version of Pscan, in which a *t*-test was implemented in place of the original *z*-test[57], with a *P*-value lower cutoff of 1e-5. The significant PWMs were grouped into families.

Over-represented sequence motifs in a window of 500 bp centered on the summit of BHLHE40 peaks were determined using PScan-ChIP[58], using as background 10,000 random sequences obtained from the DNaseI hypersensitivity cluster of ENCODE group downloaded from the UCSC genome browser [http://genome.ucsc.edu/]. Moreover, the top significant 50 PWMs of bHLH transcription factor-family were clustered based on the sequencing similarities by STAMP web server[59] and the relative phylogenetic tree visualization was performed using iTOL version 3[60].

iv) Genome browser tracks—We applied RPM normalization to all datasets and tracks for visualization in the Integrative Genomics Viewer (IGV) were generated using bedGraphToBigWig tool[52, 61].

v) Computing the transcriptional landscape—Systematic delineation of coordinated changes in gene expression patterns within specific gene sets (GSs), *i.e.* pathways, was attained by applying a previously described data analysis and data visualization pipeline[62]. This includes the following principal elements: *i.* gene set-enrichment analyses (GSEA)[63]; *ii.* leading edge analyses to handle redundancies within GSs and reduce noise; *iii.* MCL clustering for simulating the stochastic flow within the networks; *iv.* calculation of network centralities; and *v.* layout algorithms specifically developed to be used in combination with the network-analysis and visualization suite Cytoscape[64]. RNAseq data were ranked according to the FDR and the GS collection was compiled according to

Europe PMC Funders Author Manuscripts

Europe PMC Funders Author Manuscripts

Ref.[65]. Filtering for GS-size was set to larger than 10 and smaller than 500 (8095 out of 25127 GSs retained) and the connectivity threshold to connect two nodes in the network is 0.05. The network is based on the yFiles organic layout[64] and settings for MCL clustering were connectivity as array source and 2.0 as granularity parameter. All other parameters were default.

Nanostring Sprint profiling

For gene expression analysis, T cells were stimulated for 3h with PMA and ionomycin. Purified RNA (50 ng) was hybridized to the nCounter Human Immunology v2 Panel codeset. Reads were normalized using positive controls and housekeeping genes. Ratios and p-values were calculated with the nSolver 3.0 software. For miRNA expression analysis, 100 ng of total RNA were used in the Human v3 miRNA Assay. Data was normalized to spiked-in positive controls and to the 25 most highly expressed miRNAs.

Quantitative RT-PCR

Total RNA was extracted using TRI reagent (MRC) and retrotranscribed either with the qScript cDNA SuperMix (Quanta Biosciences), or the TaqMan MicroRNA Reverse Transcription Kit (Applied Biosystems). For qPCRs, the PerfeCTa SYBR Green FastMix (Quanta Bioscience) was used together with the primers for the gene targets listed in Suppl. Table 9. Taqman qPCRs were performed with the TaqMan Universal PCR Master Mix (Applied Biosystems, probes listed in Suppl. Table 9). PCR reactions were run on the ABI 79000HT Fast Real-Time PCR System (Applied Biosystems).

Transfections and transductions

Primary T cells were transfected with a miR-146a mimic oligonucleotide or a control oligonucleotide using the 100 μl Neon Transfection System kit. Briefly, 2-3 × 10^6 freshly isolated resting T cells were transfected with oligonucleotides at a final concentration of 2 μM (2200 V, 20 ms 1 pulse) and incubated for 48 h before performing subsequent analyses. HEK293 cells were cultured in 6-well plates (for luciferase reporter assays) or in T75 flasks (for production of lentiviruses). Cells were transfected with polyethylenimine (PEI) using standard protocols. Lentiviral particles were generated and purified from transfected HEK293 cells with sucrose gradient centrifugation using standard protocols. Activated primary T cells were transduced with 5-15 μl of lentiviral-containing medium in a 96-well plate with 1.5 × 10^5 cells/well. After 48-72h, transduced cells were selected by the addition of puromycin (2 μg/mL) for 48h or sorted for GFP expression, depending on the selection marker.

Plasmids

Plasmids were generated using standard cloning techniques. BHLHE40 was subcloned from a BHLHE40 vector (ABM, LV089481) into either pScalps (Addgene number 99636) or pLVX-EF1α-IRES-ZsGreen1 (Clontech). For the truncated version of BHLHE40 lacking the C-terminal domain, site-directed mutagenesis (QuikChange II XL Site-Directed Mutagenesis Kit, Agilent Technologies) was performed to introduce a stop codon at amino acid 297. A Flag-HA-tagged version of BHLHE40 was generated by inserting an N-terminal

Europe PMC Funders Author Manuscripts

Europe PMC Funders Author Manuscripts

tag. The luciferase reporter plasmid containing 4× BHLHE40 consensus binding-sites was generated by PCR amplification of synthetic oligonucleotides and cloning into the pGL3-Luciferase-promoter vector (Promega). The miR-146a sponge construct was designed based on the mature miR-146a sequence, with the addition of a central bulged mismatch. Partially overlapping forward and reverse primers were used as template for a concameric PCR as described[66]. The final PCR product was cloned downstream the mCherry reporter gene into a dual-reporter lentiviral vector. The luciferase reporter plasmid containing the -285 to +349 region surrounding the *ZC3H12D* TSS was generated by PCR amplification from gDNA and cloned upstream the luciferase gene. The corresponding plasmid containing mutations in two putative BHLHE40 binding sites was generated using the QuikChange II XL Site-Directed Mutagenesis Kit (Agilent Technologies). The luciferase reporter plasmids containing the full-length 3′UTR of the cytokines IL-22 and TNF were generated by PCR amplification from gDNA and cloning downstream the luciferase reporter gene in the pmirGLO vector. All vectors were verified by sequencing.

Reporter assays

HEK293 cells were cultured in 6-well-plates and transfected with PEI and a mix of plasmid containing the BHLHE40-expressing vector, the pGL3 luciferase reporter plasmid and a TK-Renilla plasmid with a ratio of 20:1:1. After 48 h cells were lysed using the passive lysis buffer (Dual-Luciferase® Reporter Assay System, Promega), and luciferase and renilla activities were measured according to the assay's manual using a GloMax Discover (Promega).

Immunoblots

Cells were lysed in RIPA buffer (10 mM Tris-Cl (pH 8.0), 1 mM EDTA, 1% Triton X-100, 0.1% sodium deoxycholate, 0.1% SDS, 140 mM NaCl) supplemented with a cocktail of protease inhibitors (Sigma, P8340). Protein concentration was determined with a BCA assay (Thermo Fisher, Pierce BCA Protein Assay Kit) and 25-100 μg of protein extract were loaded on a 12% polyacrylamide gel. Blotting on a PVDF membrane was performed using a methanol-based transfer buffer (20 mM Tris, 150 mM glycine, 20% methanol). Membranes were blocked with 10% milk and incubated with primary antibodies at 4°C, followed by development with HRP-conjugated secondary antibodies. Quantification was performed with a GE Amersham Imager 680.

Statistical analysis

Statistical analysis was performed with Prism software (GraphPad).

Extended Data

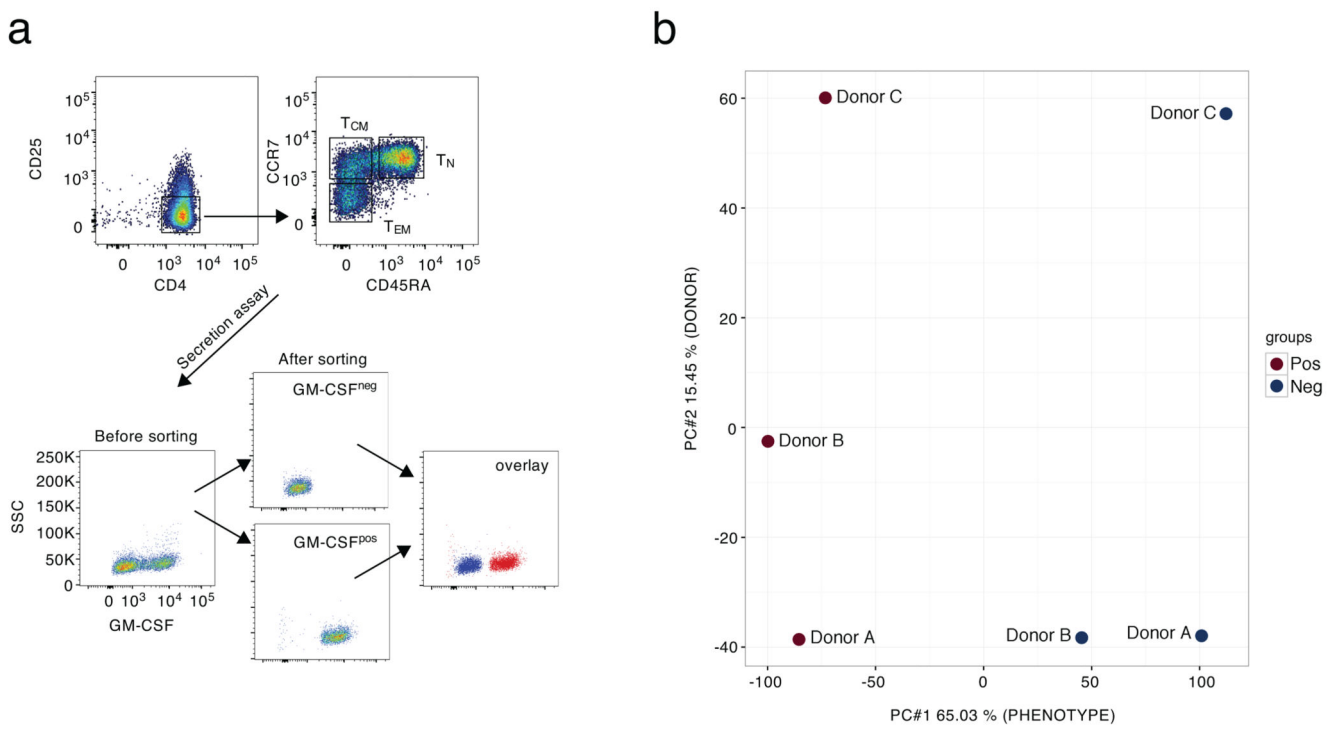

Extended Data Fig. 1. Sorting scheme and principal component analysis.

a) Sorting scheme for GM-CSF secretion assay. T_{EM} cells were separated by sorting and further divided by secretion assay and sorting. **b) Principal component analysis of RNA-seq data.** Cells from nine individual donors were separated by GM-CSF secretion assay and pooled in three pools of three donors each prior to RNA-seq. The PCA analysis showed robust results, with differences due to sample-to-sample variability accounting for only 15.45% (PC#2) of the variance, while the majority of the observed differences were due to the phenotype of the cells (65.03%, GM-CSFpos *vs.* neg, PC#1).

Europe PMC Funders Author Manuscripts
Europe PMC Funders Author Manuscripts

Europe PMC Funders Author Manuscripts

Europe PMC Funders Author Manuscripts

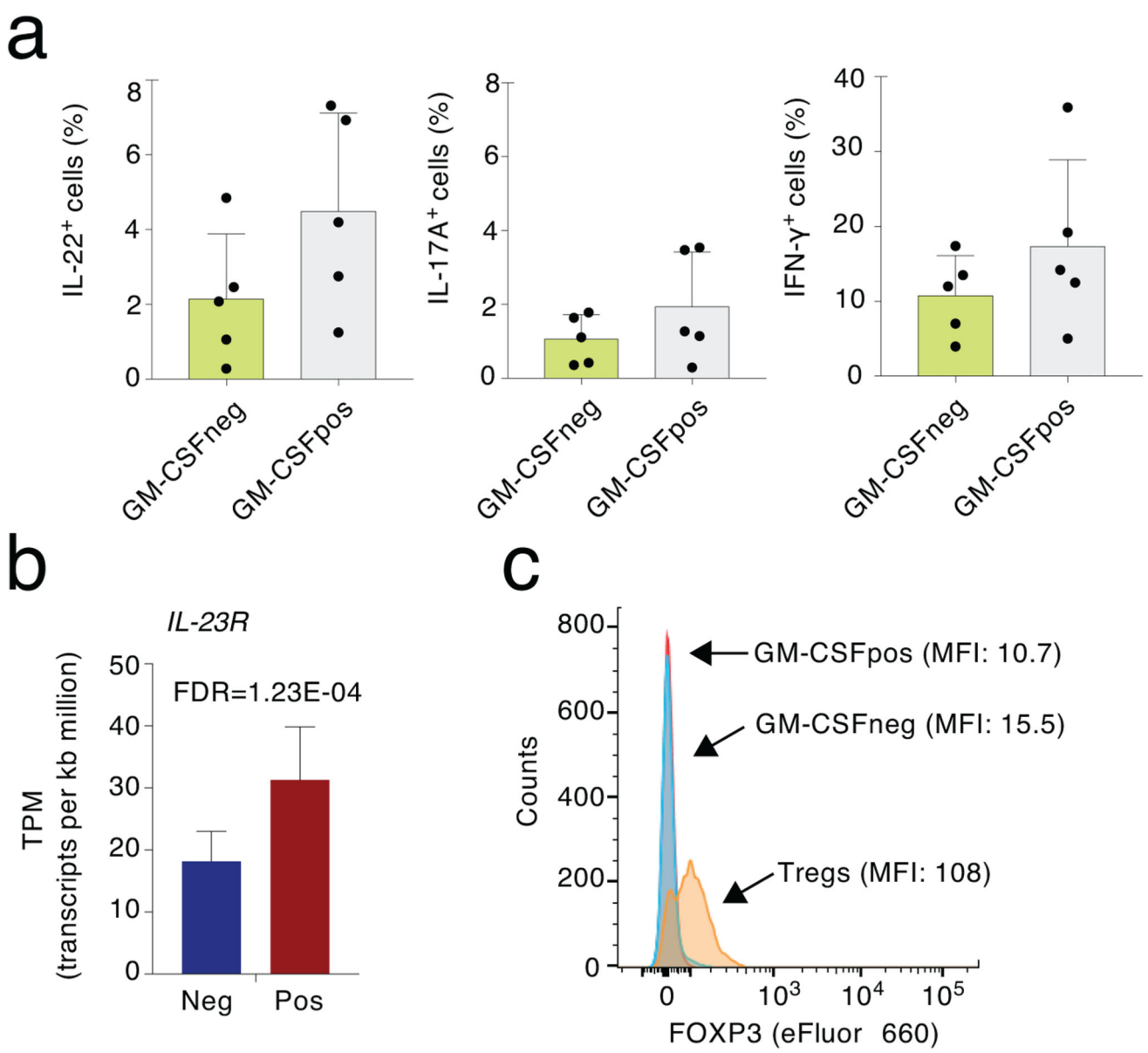

Extended Data Fig. 2. Expression of specific markers in T cell subsets.

a) Cytokine expression in different T cell subsets. Each indicated cytokine (IL-22, IL-17A and IFN-γ is expressed with or without concomitant co-expression of GM-CSF. Also, the IL-22pos cells are not simply a subset of the larger GM-CSFpos pool of cells. Mean ± SD. Each dot represents one donor (n=5). **b) Expression of *IL23R*.** Expression of the *IL23R* gene in GM-CSFpos and GM-CSFneg cells, as determined by RNA-seq (n=9). FDR=False discovery rate calculated for RNA-seq samples. **c) FOXP3 expression.** Comparison of FOXP3 expression in Treg cells ($CD4^{+}CD25^{high}CD127^{low}$), GM-CSFpos and GM-CSFneg cells, as assessed by intracellular staining. Representative of n=2 experiments.

Europe PMC Funders Author Manuscripts

Europe PMC Funders Author Manuscripts

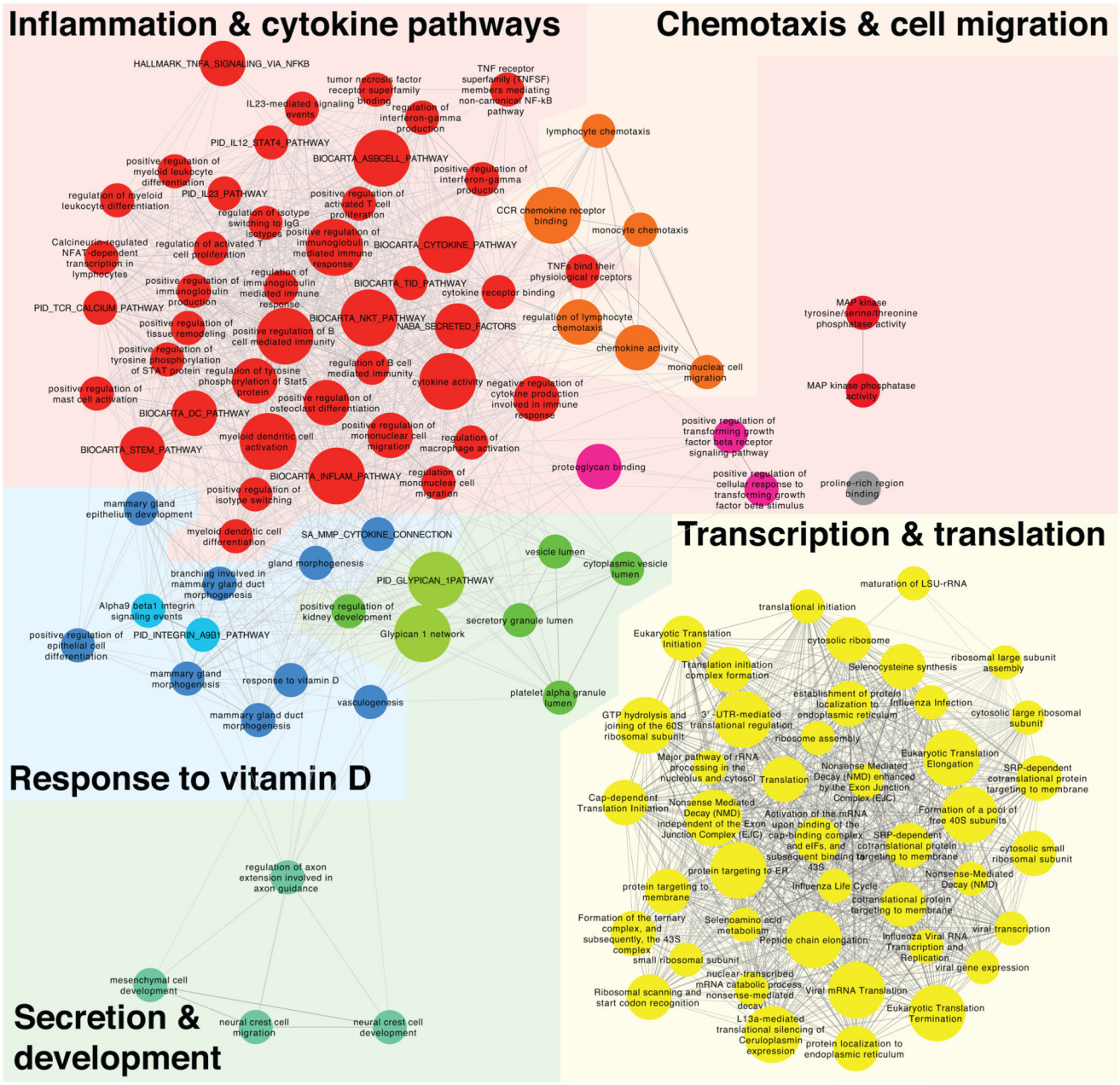

Extended Data Fig. 3. Differences in gene expression patterns between GM-CSF^{+} and GM-CSF^{-} T_{EM} cells

Systematic delineation of coordinated changes in gene expression within specific gene sets, *i.e.* pathways, was achieved by applying the data analysis and data visualization pipeline described in the Methods. 119 gene sets yielded significant enrichment in GM-CSFpos *vs.* GM-CSFneg cells (false-discovery-rate (FDR)-q <0.01, nom. p-value of < 0.005 and TAGS >50) whereas none were found depleted. Defining the network's organization is the degree of overlap in leading edge-genes (genes contributing to each gene set's significant enrichment) two gene sets (nodes) linked by a connection (edge) share (threshold connectivity 0.05). Node-size corresponds to FDR-q value threshold passed by the gene set

(small < 0.01, medium < 0.001, large < 0.0001). Node color denotes MCL-cluster membership that subsequently would be summarized within 5 biological themes *i.e.* color-coded network areas. Their FDR-*q* value distribution is displayed in Figure 1f.

Europe PMC Funders Author Manuscripts

Europe PMC Funders Author Manuscripts

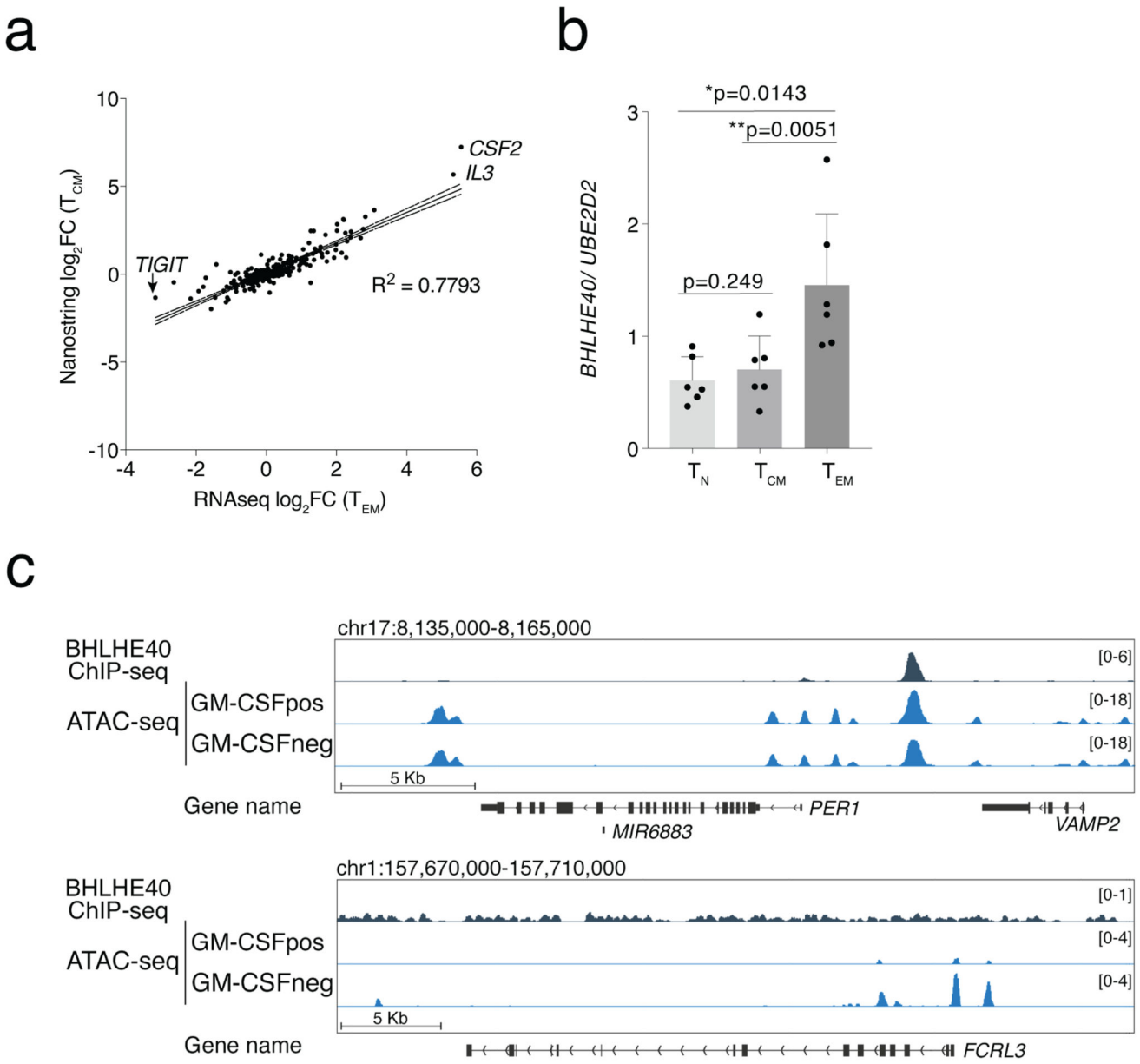

Extended Data Fig. 4. RNA-seq, Nanostring, ATAC-seq and ChIP-seq analyses.

a) Comparison of RNA-seq and Nanostring data. Concordant results of gene expression profiling obtained by RNA-seq of T_{EM} cells and Nanostring profiling of T_{CM} cells. **b) Expression of *BHLHE40* in different T cell subsets.** Expression of *BHLHE40* was determined by qRT-PCR in different T cell subsets freshly sorted from peripheral blood. Each dot represents one donor (n=6). Mean ± SD; paired t-test, two-tailed. **c) ATAC-seq and ChIP-seq analyses.** Representative snapshots of ChIP-seq and ATAC-seq tracks for selected genomic loci.

Europe PMC Funders Author Manuscripts
Europe PMC Funders Author Manuscripts

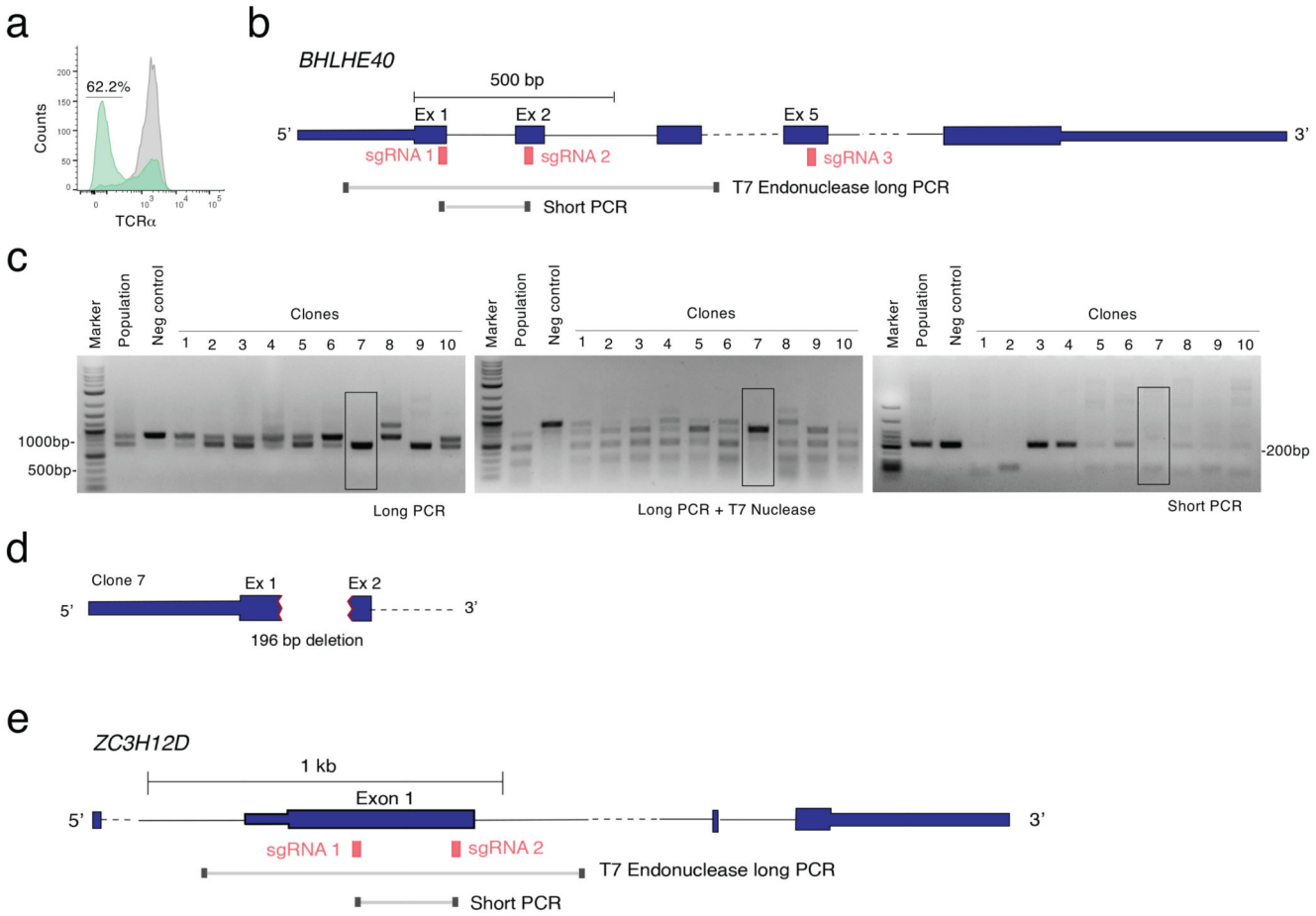

Extended Data Fig. 5. Optimization of CRISP-Cas9-mediated deletion and screening.

a) As a proof-of-principle and test of efficiency, Jurkat T cells were transfected using the Neon transfection system with ribonucleoparticles of Cas9 and one single guide RNA against the TCRα chain. After three days the cells were stained for surface TCR expression, showing a loss of expression in 62% of the cells (green). Grey: mock transfected control cells. Representative of at least n=3 independent experiments. **b)** Schematic representation of the *BHLHE40* locus with indicated the location of guide RNAs and primers used for screening of the clones. **c)** Optimization of screening procedure by mismatch cleavage assay. After transfection with two guide RNAs against *BHLHE40*, Jurkat cells were single cell-cloned by seeding in a 384-well plate in 20% FBS. Genomic DNA was extracted from 10 clones and from the entire population (no cloning) and negative controls. The first 'long' PCR showed already the presence of indels in most clones (left panel) and even at the level of whole population. This was further confirmed by denaturing, reannealing and T7 endonuclease digestion (middle panel). The presence of a homozygous deletion was further confirmed using a 'short' PCR that cannot provide an amplification product if the region between the two guide RNAs is deleted. The highlighted Clone 7 (black box) is one of several clones in which the deletion was most likely identical on both alleles, leading to a shorter PCR product that cannot be digested by the T7 endonuclease because of the absence of mismatches. Representative of at least n=2 independent transfections and cloning

Europe PMC Funders Author Manuscripts
Europe PMC Funders Author Manuscripts

procedures. **d)** The genomic DNA from Clone 7 was sequenced in the *BHLHE40* locus region, revealing a deletion of 196 nucleotides involving part of exon 1 and exon 2, as well as the intron. **e)** Schematic representation of the *ZC3H12D* locus with indicated the location of guide RNAs and primers used for screening of the clones in Figure 8f.

Europe PMC Funders Author Manuscripts

Europe PMC Funders Author Manuscripts

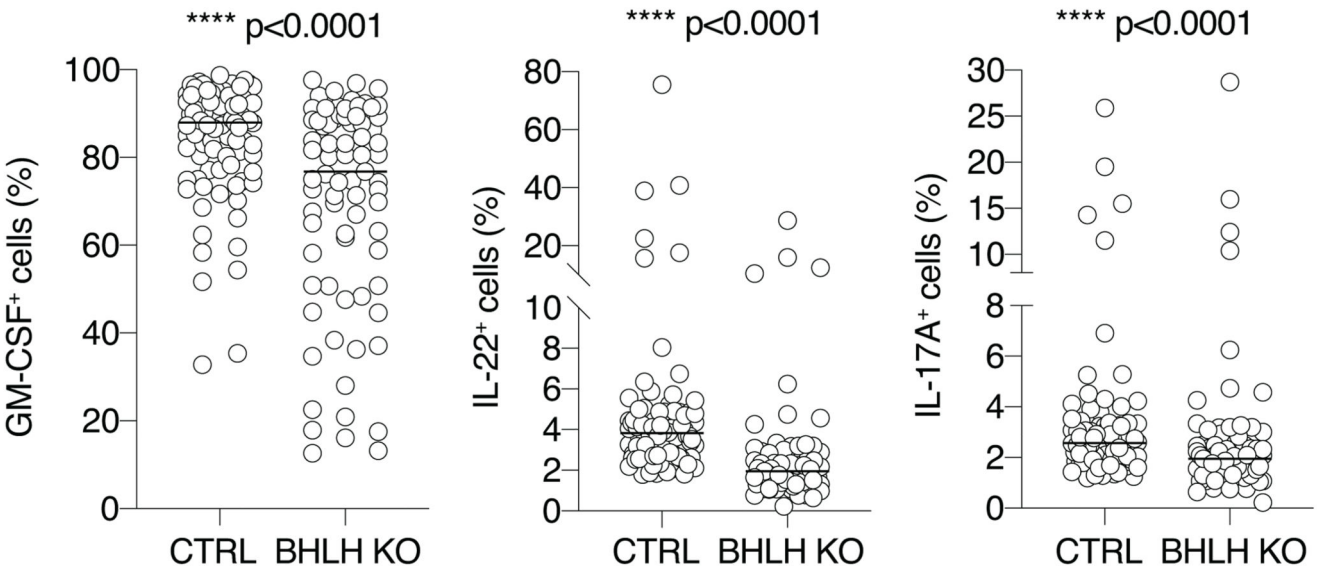

Extended Data Fig. 6. Analysis of primary human T cell clones transfected with Cas9 ribonucleoparticles directed against the *BHLHE40* gene.

Primary human memory T lymphocytes were transfected with ribonucleoparticles of Cas9 and gRNAs against exon 1/2 and exon 5 of *BHLHE40*. After single cell cloning and expansion, individual clones were tested for the presence of the deletion by PCR. Median; Mann-Whitney test. Each dot represents one clone (n=77 for KO and n=90 for control clones).

Europe PMC Funders Author Manuscripts
Europe PMC Funders Author Manuscripts

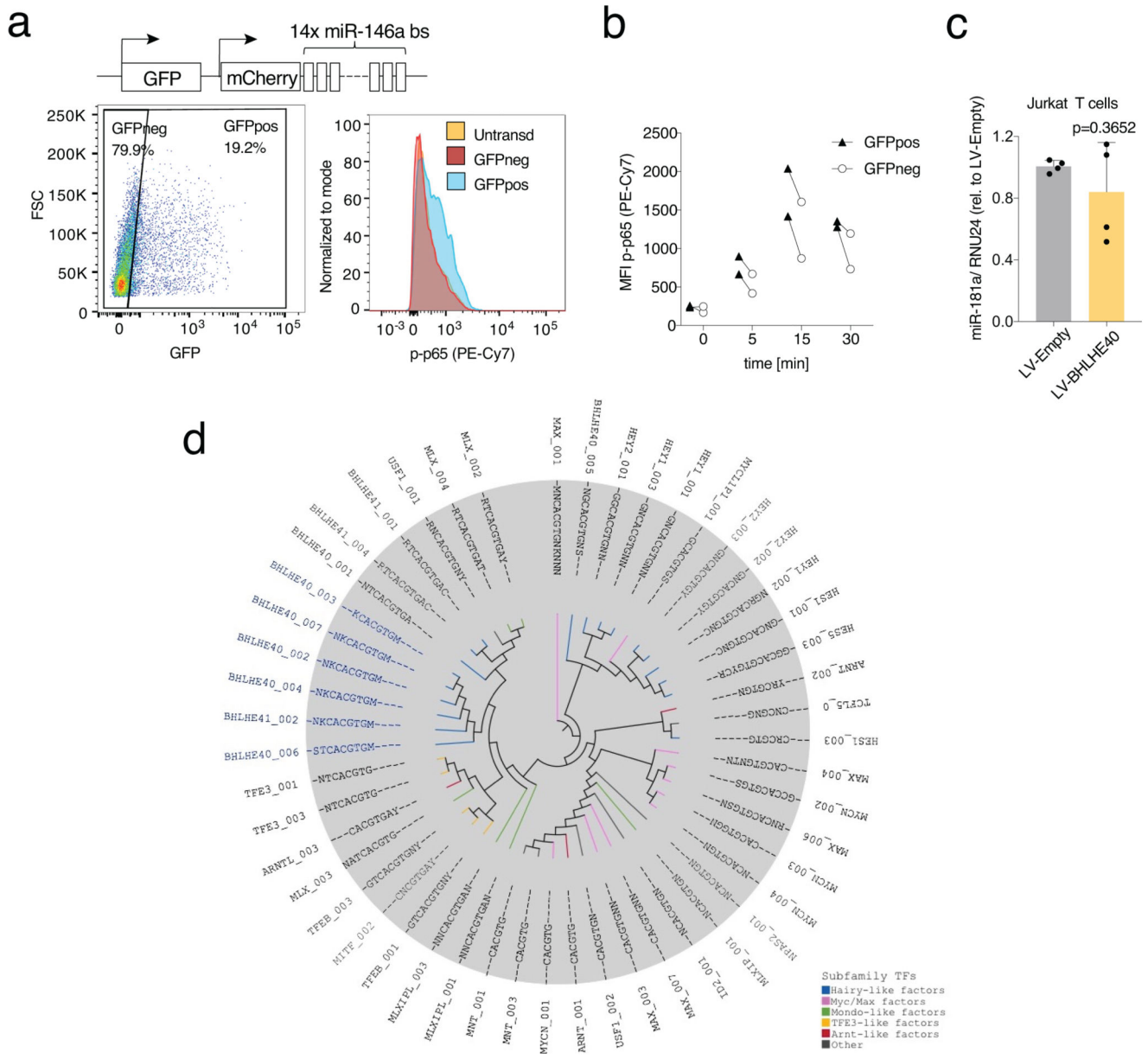

Extended Data Fig. 7. MiRNA analysis.

a) Transduction with a miR-146a sponge of primary human T lymphocytes leads to increased NF-kB p65 phosphorylation. Primary memory T lymphocytes were transduced with a lentivirus expressing a miR-146a sponge and GFP as an independent reporter of the efficiency of transduction (schematic representation on top); a few days after transduction cells were stimulated with PMA and ionomycin for 5 minutes and levels of p65 phosphorylation were determined by intracellular staining. Cells were gated as GFPneg (non-expressing the sponge) and GFPpos (expressing the sponge) and compared also to untransduced cells. Representative of n=2 experiments. **b)** Same as c) expect that the results (expressed as mean fluorescence intensity) of two independent experiments in which cells were stimulated for the indicated times are shown. **c) Effect of BHLHE40 expression on**

Europe PMC Funders Author Manuscripts
Europe PMC Funders Author Manuscripts

miR-181a in Jurkat T cells. Jurkat T cells were transduced with a BHLHE40-expressing lentivirus. After selection and expansion of the transduced cells, expression of miR-181a was measured by qRT-PCR. Each dot represents one independent experiment (n=4). Mean ± SD; paired t-test, two-tailed. **d)** Phylogenetic analysis of the top 50 bHLH matrices recovered from the BHLHE40 ChIP-seq data.

Europe PMC Funders Author Manuscripts

Europe PMC Funders Author Manuscripts

Europe PMC Funders Author Manuscripts

Europe PMC Funders Author Manuscripts

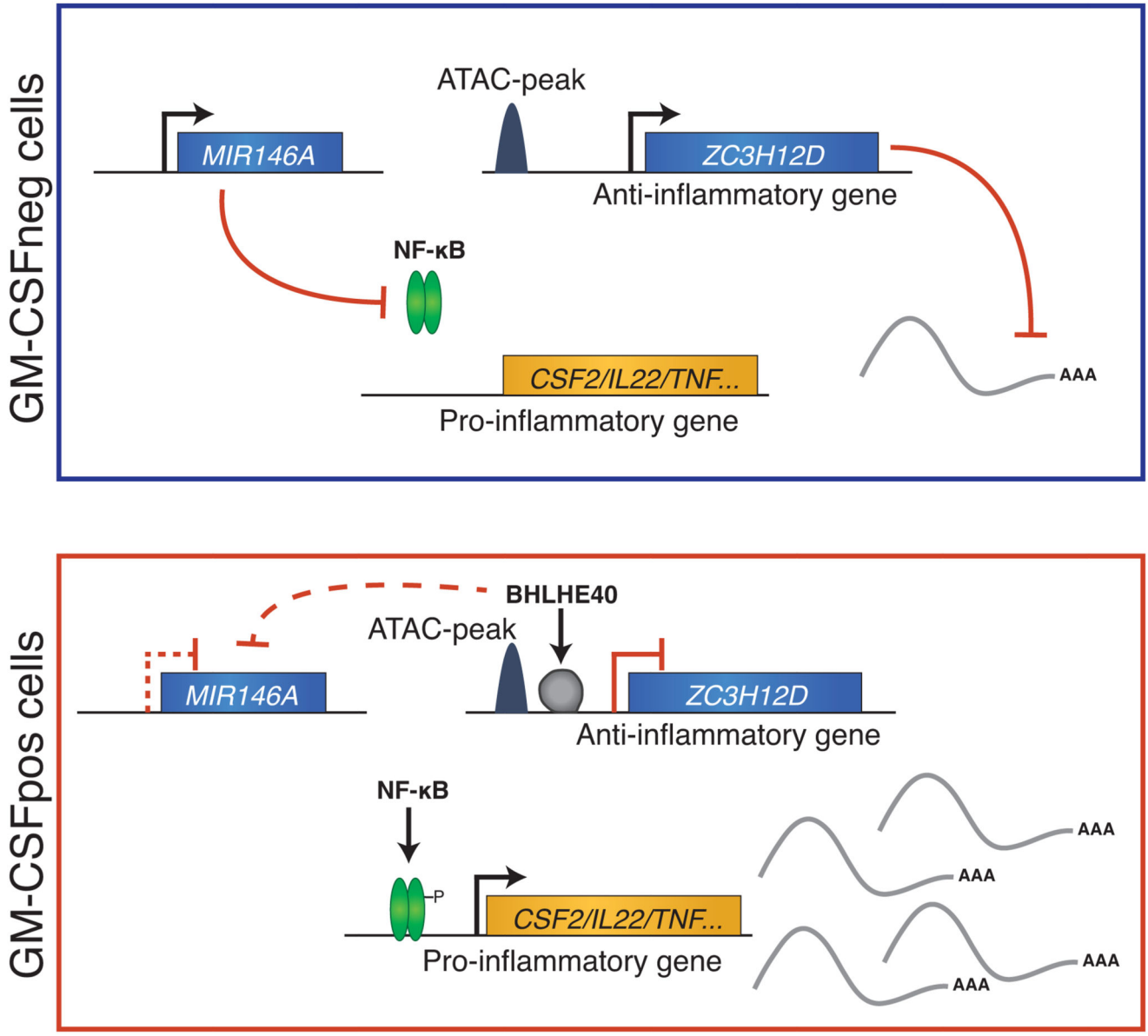

Extended Data Fig. 8. Schematic diagram describing the regulatory module identified in this study.

Using GM-CSF secretion as a proxy for an inflammatory phenotype of primary human memory T_H lymphocytes, we identified a regulatory module that influences the activity of these pro-inflammatory and potentially pathogenic cells. In GM-CSF$^-$ cells, mechanisms are in place to actively repress the expression of inflammatory cytokines, including high levels of miR-146a expression (a negative regulator of NF-κB activation), and relatively higher expression of *ZC3H12D*, an RNase enzyme involved in the negative regulation of cytokine expression. Conversely, in GM-CSF$^+$ cells, the expression of the transcriptional repressor BHLHE40 leads to the direct downregulation of *ZC3H12D* expression, and indirectly affects also miR-146a. This in turn allows full-blown NF-κB activation and expression of inflammatory cytokines.

Supplementary Material

Refer to Web version on PubMed Central for supplementary material.

Acknowledgements

The authors would like to thank D. Jarossay, S. Notarbartolo and F. Mele for invaluable technical support and input, M. Perez for help with Figure 1, L. Vincenzetti for pilot CRISPR-Cas9 experiments and E. Džafo for help with experiments involving Regnase-4. This work was supported by the Swiss National Science Foundation (grant number 156875 and 175569), the NCCR 'RNA & Disease', the Swiss MS Society, the Ceresio Foundation, the Vontobel Stiftung and the Kurt und Senta Herrmann Stiftung (all to S.M.). S. Montagner was supported by a Marie Heim-Vögtlin postdoctoral fellowship (number 164489).

References

1. Newell EW, Sigal N, Bendall SC, Nolan GP, Davis MM. Cytometry by time-of-flight shows combinatorial cytokine expression and virus-specific cell niches within a continuum of CD8+ T cell phenotypes. Immunity. 2012; 36:142–152. [PubMed: 22265676]
2. Helmstetter C, et al. Individual T helper cells have a quantitative cytokine memory. Immunity. 2015; 42:108–122. [PubMed: 25607461]
3. Cao Y, et al. Functional inflammatory profiles distinguish myelin-reactive T cells from patients with multiple sclerosis. Sci Transl Med. 2015; 7
4. Galli E, et al. GM-CSF and CXCR4 define a T helper cell signature in multiple sclerosis. Nat Med. 2019; 25:1290–1300. [PubMed: 31332391]
5. Hartmann FJ, et al. Multiple sclerosis-associated IL2RA polymorphism controls GM-CSF production in human TH cells. Nature Commun. 2014; 5
6. Hirota K, et al. Autoimmune Th17 Cells Induced Synovial Stromal and Innate Lymphoid Cell Secretion of the Cytokine GM-CSF to Initiate and Augment Autoimmune Arthritis. Immunity. 2018; 48:1220–1232 e1225. [PubMed: 29802020]
7. Behrens F, et al. MOR103, a human monoclonal antibody to granulocyte-macrophage colony-stimulating factor, in the treatment of patients with moderate rheumatoid arthritis: results of a phase Ib/IIa randomised, double-blind, placebo-controlled, dose-escalation trial. Ann Rheum Dis. 2015; 74:1058–1064. [PubMed: 24534756]
8. Burmester GR, et al. Efficacy and safety of mavrilimumab in subjects with rheumatoid arthritis. Ann Rheum Dis. 2013; 72:1445–1452. [PubMed: 23234647]
9. de Vries EG, et al. Flare-up of rheumatoid arthritis during GM-CSF treatment after chemotherapy. Lancet. 1991; 338:517–518.
10. Codarri L, et al. RORgammat drives production of the cytokine GM-CSF in helper T cells, which is essential for the effector phase of autoimmune neuroinflammation. Nat Immunol. 2011; 12:560–567. [PubMed: 21516112]
11. Sonderegger I, et al. GM-CSF mediates autoimmunity by enhancing IL-6-dependent Th17 cell development and survival. J Exp Med. 2008; 205:2281–2294. [PubMed: 18779348]
12. McQualter JL, et al. Granulocyte macrophage colony-stimulating factor: a new putative therapeutic target in multiple sclerosis. J Exp Med. 2001; 194:873–882. [PubMed: 11581310]
13. Campbell IK, et al. Protection from collagen-induced arthritis in granulocyte-macrophage colony-stimulating factor-deficient mice. J Immunol. 1998; 161:3639–3644. [PubMed: 9759887]
14. Wawro M, Kochan J, Krzanik S, Jura J, Kasza A. Intact NYN/PIN-Like Domain is Crucial for the Degradation of Inflammation-Related Transcripts by ZC3H12D. J Cell Biochem. 2017; 118:487–498. [PubMed: 27472830]
15. Taganov KD, Boldin MP, Chang KJ, Baltimore D. NF-kappaB-dependent induction of microRNA miR-146, an inhibitor targeted to signaling proteins of innate immune responses. Proc Natl Acad Sci USA. 2006; 103:12481–12486. [PubMed: 16885212]

Europe PMC Funders Author Manuscripts
Europe PMC Funders Author Manuscripts

Europe PMC Funders Author Manuscripts

16. McGeachy MJ, et al. The interleukin 23 receptor is essential for the terminal differentiation of interleukin 17-producing effector T helper cells in vivo. Nat Immunol. 2009; 10:314–324. [PubMed: 19182808]
17. Sakaguchi S, Miyara M, Costantino CM, Hafler DA. FOXP3+ regulatory T cells in the human immune system. Nat Rev Immunol. 2010; 10:490–500. [PubMed: 20559327]
18. Ascherio A, Munger KL, Simon KC. Vitamin D and multiple sclerosis. Lancet Neurol. 2010; 9:599–612. [PubMed: 20494325]
19. Kongsbak M, Levring TB, Geisler C, von Essen MR. The vitamin d receptor and T cell function. Front Immunol. 2013; 4:148. [PubMed: 23785369]
20. Annunziato F, et al. Phenotypic and functional features of human Th17 cells. J Exp Med. 2007; 204:1849–1861. [PubMed: 17635957]
21. Lin CC, et al. IL-1-induced Bhlhe40 identifies pathogenic T helper cells in a model of autoimmune neuroinflammation. J Exp Med. 2016; 213:251–271. [PubMed: 26834156]
22. Sun H, Lu B, Li RQ, Flavell RA, Taneja R. Defective T cell activation and autoimmune disorder in Stra13-deficient mice. Nat Immunol. 2001; 2:1040–1047. [PubMed: 11668339]
23. Martinez-Llordella M, et al. CD28-inducible transcription factor DEC1 is required for efficient autoreactive CD4+ T cell response. J Exp Med. 2013; 210:1603–1619. [PubMed: 23878307]
24. Lin CC, et al. Bhlhe40 controls cytokine production by T cells and is essential for pathogenicity in autoimmune neuroinflammation. Nat Commun. 2014; 5
25. Huynh JP, et al. Bhlhe40 is an essential repressor of IL-10 during Mycobacterium tuberculosis infection. J Exp Med. 2018; 215:1823–1838. [PubMed: 29773644]
26. Yu F, et al. The transcription factor Bhlhe40 is a switch of inflammatory versus antiinflammatory Th1 cell fate determination. J Exp Med. 2018; 215:1813–1821. [PubMed: 29773643]
27. Miyazaki K, et al. The role of the basic helix-loop-helix transcription factor Dec1 in the regulatory T cells. J Immunol. 2010; 185:7330–7339. [PubMed: 21057086]
28. Ran FA, et al. Genome engineering using the CRISPR-Cas9 system. Nat Protoc. 2013; 8:2281–2308. [PubMed: 24157548]
29. Geiger R, Duhen T, Lanzavecchia A, Sallusto F. Human naive and memory CD4+ T cell repertoires specific for naturally processed antigens analyzed using libraries of amplified T cells. J Exp Med. 2009; 206:1525–1534. [PubMed: 19564353]
30. Mele F, et al. ERK phosphorylation and miR-181a expression modulate activation of human memory TH17 cells. Nat Commun. 2015; 6
31. St-Pierre B, Flock G, Zacksenhaus E, Egan SE. Stra13 homodimers repress transcription through class B E-box elements. J Biol Chem. 2002; 277:46544–46551. [PubMed: 12297495]
32. Sun H, Taneja R. Stra13 expression is associated with growth arrest and represses transcription through histone deacetylase (HDAC)-dependent and HDAC-independent mechanisms. Proc Natl Acad Sci USA. 2000; 97:4058–4063. [PubMed: 10737769]
33. Ivanova AV, et al. STRA13 interacts with STAT3 and modulates transcription of STAT3-dependent targets. J Mol Biol. 2004; 340:641–653. [PubMed: 15223310]
34. Li Y, et al. DEC1 negatively regulates the expression of DEC2 through binding to the E-box in the proximal promoter. J Biol Chem. 2003; 278:16899–16907. [PubMed: 12624110]
35. Housley WJ, et al. Genetic variants associated with autoimmunity drive NFkappaB signaling and responses to inflammatory stimuli. Sci Transl Med. 2015; 7
36. Monticelli S, Aijo T, Trifari S. Approaches to Detect microRNA Expression in T Cell Subsets and T Cell Differentiation. Methods Mol Biol. 2017; 1514:153–172. [PubMed: 27787800]
37. Matsushita K, et al. Zc3h12a is an RNase essential for controlling immune responses by regulating mRNA decay. Nature. 2009; 458:1185–1190. [PubMed: 19322177]
38. Liang J, et al. MCP-induced protein 1 deubiquitinates TRAF proteins and negatively regulates JNK and NF-kappaB signaling. J Exp Med. 2010; 207:2959–2973. [PubMed: 21115689]
39. Minagawa K, et al. Posttranscriptional modulation of cytokine production in T cells for the regulation of excessive inflammation by TFL. J Immunol. 2014; 192:1512–1524. [PubMed: 24415781]

Europe PMC Funders Author Manuscripts

40. Ferber IA, et al. Mice with a disrupted IFN-gamma gene are susceptible to the induction of experimental autoimmune encephalomyelitis (EAE). J Immunol. 1996; 156:5–7. [PubMed: 8598493]
41. Bettelli E, et al. Loss of T-bet, but not STAT1, prevents the development of experimental autoimmune encephalomyelitis. J Exp Med. 2004; 200:79–87. [PubMed: 15238607]
42. Oestreich KJ, Weinmann AS. Master regulators or lineage-specifying? Changing views on CD4+ T cell transcription factors. Nat Rev Immunol. 2012; 12:799–804. [PubMed: 23059426]
43. Kanda M, et al. Transcriptional regulator Bhlhe40 works as a cofactor of T-bet in the regulation of IFN-gamma production in iNKT cells. Proc Natl Acad Sci USA. 2016; 113:E3394–3402. [PubMed: 27226296]
44. Zhang L, et al. Lineage tracking reveals dynamic relationships of T cells in colorectal cancer. Nature. 2018; 564:268–272. [PubMed: 30479382]
45. Hosokawa H, et al. Transcription Factor PU.1 Represses and Activates Gene Expression in Early T Cells by Redirecting Partner Transcription Factor Binding. Immunity. 2018; 48:1119–1134 e1117. [PubMed: 29924977]
46. Oestreich KJ, Weinmann AS. T-bet employs diverse regulatory mechanisms to repress transcription. Trends Immunol. 2012; 33:78–83. [PubMed: 22133865]
47. Curina A, et al. High constitutive activity of a broad panel of housekeeping and tissue-specific cis-regulatory elements depends on a subset of ETS proteins. Genes Dev. 2017; 31:399–412. [PubMed: 28275002]
48. Balestrieri C, et al. Co-optation of Tandem DNA Repeats for the Maintenance of Mesenchymal Identity. Cell. 2018; 173:1150–1164 e1114. [PubMed: 29706544]
49. Bolger AM, Lohse M, Usadel B. Trimmomatic: a flexible trimmer for Illumina sequence data. Bioinformatics. 2014; 30:2114–2120. [PubMed: 24695404]
50. Buenrostro JD, Giresi PG, Zaba LC, Chang HY, Greenleaf WJ. Transposition of native chromatin for fast and sensitive epigenomic profiling of open chromatin, DNA-binding proteins and nucleosome position. Nat Methods. 2013; 10:1213–1218. [PubMed: 24097267]
51. Zhang Y, et al. Model-based analysis of ChIP-Seq (MACS). Genome Biol. 2008; 9
52. Quinlan AR, Hall IM. BEDTools: a flexible suite of utilities for comparing genomic features. Bioinformatics. 2010; 26:841–842. [PubMed: 20110278]
53. Ross-Innes CS, et al. Differential oestrogen receptor binding is associated with clinical outcome in breast cancer. Nature. 2012; 481:389–393. [PubMed: 22217937]
54. Heinz S, et al. Simple combinations of lineage-determining transcription factors prime cis-regulatory elements required for macrophage and B cell identities. Mol Cell. 2010; 38:576–589. [PubMed: 20513432]
55. McLean CY, et al. GREAT improves functional interpretation of cis-regulatory regions. Nat Biotechnol. 2010; 28:495–501. [PubMed: 20436461]
56. Diaferia GR, et al. Dissection of transcriptional and cis-regulatory control of differentiation in human pancreatic cancer. EMBO J. 2016; 35:595–617. [PubMed: 26769127]
57. Zambelli F, Pesole G, Pavesi G. Pscan: finding over-represented transcription factor binding site motifs in sequences from co-regulated or co-expressed genes. Nucleic Acids Res. 2009; 37:W247–252. [PubMed: 19487240]
58. Zambelli F, Pesole G, Pavesi G. PscanChIP: Finding over-represented transcription factor-binding site motifs and their correlations in sequences from ChIP-Seq experiments. Nucleic Acids Res. 2013; 41:W535–543. [PubMed: 23748563]
59. Mahony S, Benos PV. STAMP: a web tool for exploring DNA-binding motif similarities. Nucleic Acids Res. 2007; 35:W253–258. [PubMed: 17478497]
60. Letunic I, Bork P. Interactive tree of life (iTOL) v3: an online tool for the display and annotation of phylogenetic and other trees. Nucleic Acids Res. 2016; 44:W242–245. [PubMed: 27095192]
61. Li H, et al. The Sequence Alignment/Map format and SAMtools. Bioinformatics. 2009; 25:2078–2079. [PubMed: 19505943]

62. Delaleu N, Nguyen CQ, Tekle KM, Jonsson R, Peck AB. Transcriptional landscapes of emerging autoimmunity: transient aberrations in the targeted tissue's extracellular milieu precede immune responses in Sjogren's syndrome. Arthritis Res Ther. 2013; 15

63. Subramanian A, et al. Gene set enrichment analysis: a knowledge-based approach for interpreting genome-wide expression profiles. Proc Natl Acad Sci USA. 2005; 102:15545–15550. [PubMed: 16199517]

64. Su G, Morris JH, Demchak B, Bader GD. Biological network exploration with Cytoscape 3. Curr Protoc Bioinformatics. 2014; 47

65. Merico D, Isserlin R, Stueker O, Emili A, Bader GD. Enrichment map: a network-based method for gene-set enrichment visualization and interpretation. PloS One. 2010; 5:e13984. [PubMed: 21085593]

66. Lindner SE, et al. The miR-15 family reinforces the transition from proliferation to differentiation in pre-B cells. EMBO Rep. 2017; 18:1604–1617. [PubMed: 28705801]

Europe PMC Funders Author Manuscripts

Europe PMC Funders Author Manuscripts

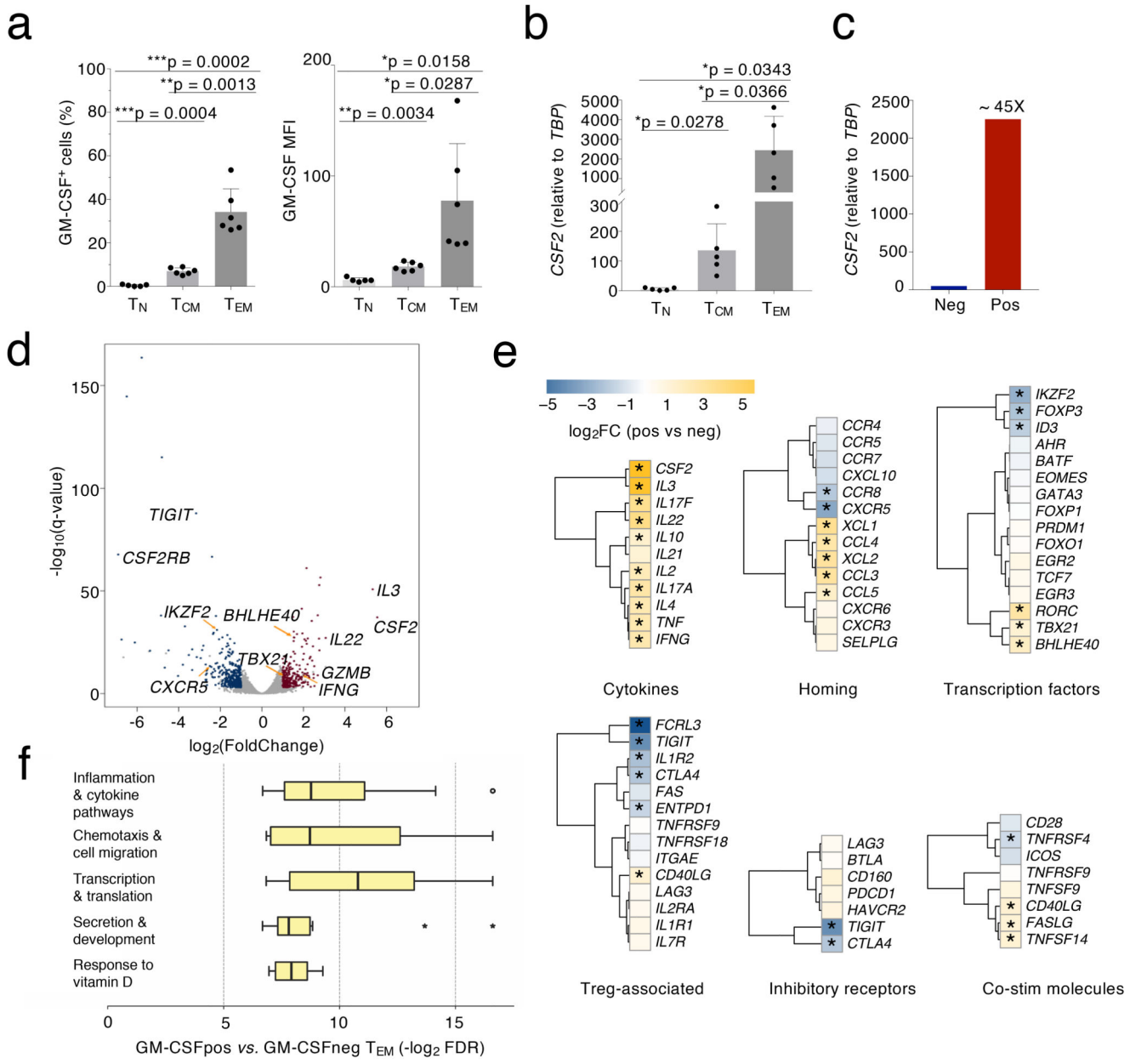

Figure 1. Transcriptomic analysis of GM-CSF$^+$ and GM-CSF$^-$ cells.

a) Overall levels of GM-CSF expression were determined by intracellular staining in different human T cell subsets (T_N, T_{CM} and T_{EM}) freshly isolated from peripheral blood. Both the percentage of positive cells (left) and the MFI (mean fluorescence intensity, right) are shown. Each dot represents one donor (n=6). Mean ± SD; paired t-test, two-tailed. **b)** Levels of *CSF2* mRNA expression were determined in the different T cell subsets by qRT-PCR. Each dot represents one donor (n=5). Mean ± SD; paired t-test, two-tailed. **c)** T_{EM} cells from n=5 donors were further separated in GM-CSF$^-$ and GM-CSF$^+$ by secretion assay and pooled. Levels of *CSF2* mRNA expression were determined by qRT-PCR. Data are representative of two independent experiments. Technical replicates are not shown. **d)** Cells

Europe PMC Funders Author Manuscripts
Europe PMC Funders Author Manuscripts

from n=9 independent donors as in c) were separated and analyzed by RNA-seq (3 pools of 3 independent donors each). Volcano plot shows the differentially expressed genes for GM-CSF^{-} *vs.* GM-CSF^{+} cells, using the likelihood ratio tests of EdgeR. Blue and red dots indicate genes up-regulated in GM-CSF^{-} and up-regulated in GM-CSF^{+} cells, respectively (FDR ≤ 0.05 and absolute $\log_2$ FC ≥ 1). All other genes are indicated as gray dots. **e)** Expression of relevant immune-related genes, as determined by RNA-seq in d). The asterisk (*) indicates genes significantly differential expressed in all samples for each condition (absolute Log_2FC≥1 FDR≤0.001 TPM≥1). **f)** FDR *q*-value distribution of significantly enriched gene sets in GM-CSF^{+} *vs.* GM-CSF^{-} T_{EM} cells clustering within specific biological themes. The transcriptional landscape underlying this panel is displayed in Extended Data 3. Each bar describes median, first and third quartiles and maximum and minimum values. Outliers (circles) and extremes (asterisks) are indicated.

Europe PMC Funders Author Manuscripts

Europe PMC Funders Author Manuscripts

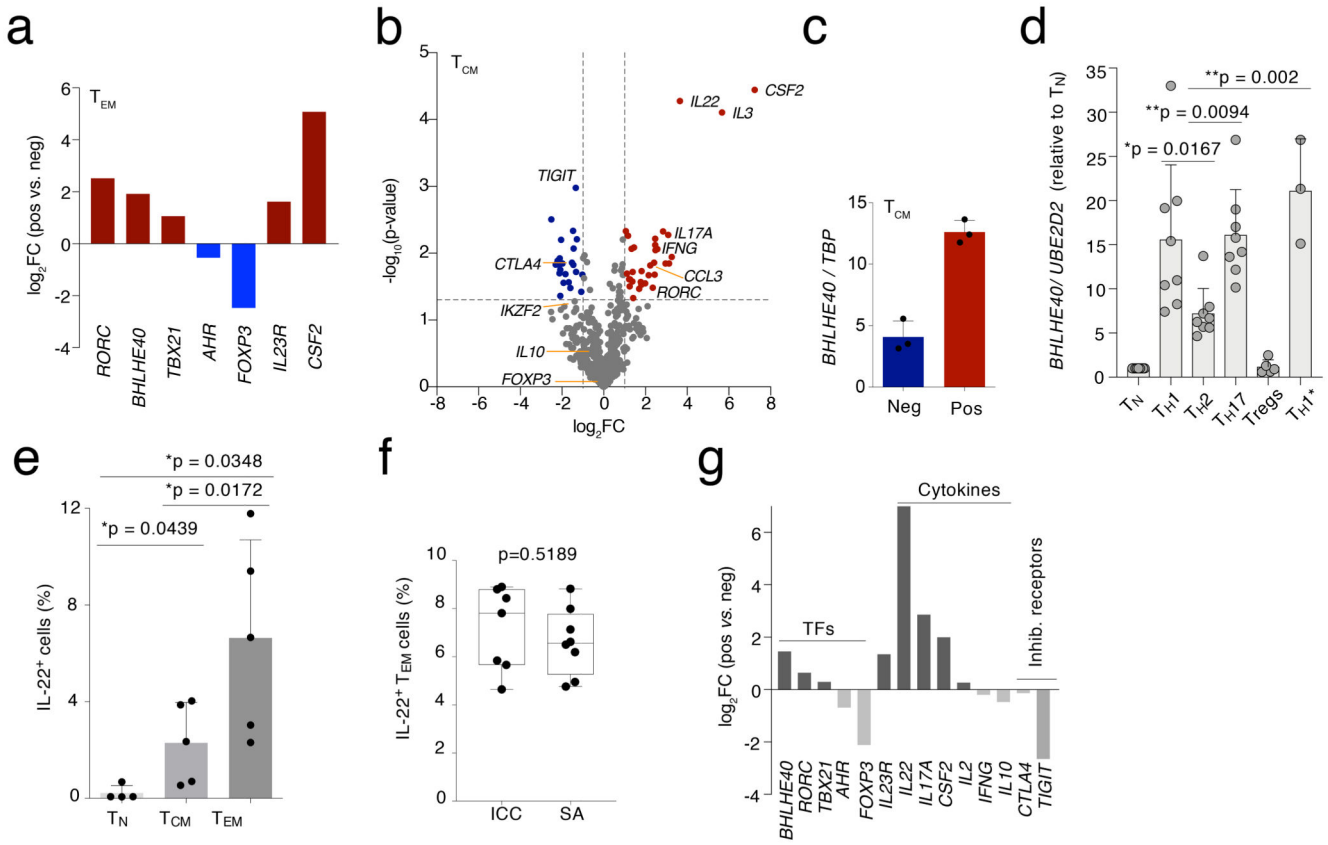

Figure 2. A general gene signature linked to a high cytokine-producing phenotype.

a) Selected differentially expressed genes identified by RNA-seq were validated by qRT-PCR on an independent pool of n=3 donors. **b)** T_{CM} cells from 3 pools of n=2 donors each were separated by GM-CSF secretion assay in GM-CSF^{+} and GM-CSF^{-} and the expression of immune-relevant genes was determined by Nanostring profiling (t-test, two-tailed). **c)** Expression of *BHLHE40* was determined by qRT-PCR in T_{CM} cells separated by GM-CSF secretion assay. Each dot represents a pool of two individual donors (n=6). **d)** Expression of *BHLHE40* in different effector T cell subsets. Each dot represents one donor (n= at least 3). Mean ± SD; one-way Anova. **e)** The overall percentage of IL-22-expressing cells was determined by intracellular staining in the different human T cell subsets. Each dot represents one donor (n=5). Mean ± SD; paired t-test, two-tailed. **f)** Comparison between the percentages of IL-22-expressing cells obtained by intracellular staining (ICC) and cytokine secretion assays (SA) of T_{EM} cells. Each dot represents one donor (n=8). Median with 95% confidence interval, min to max; paired t-test, two-tailed. **g)** Expression of selected genes was determined by qRT-PCR in T_{EM} cells separated by IL-22 secretion assay. To obtain a sufficient number of cells for RNA extraction and qRT-PCR, n=8 individual donors were pooled after IL-22 secretion assays. Technical replicates are not shown.

Europe PMC Funders Author Manuscripts
Europe PMC Funders Author Manuscripts

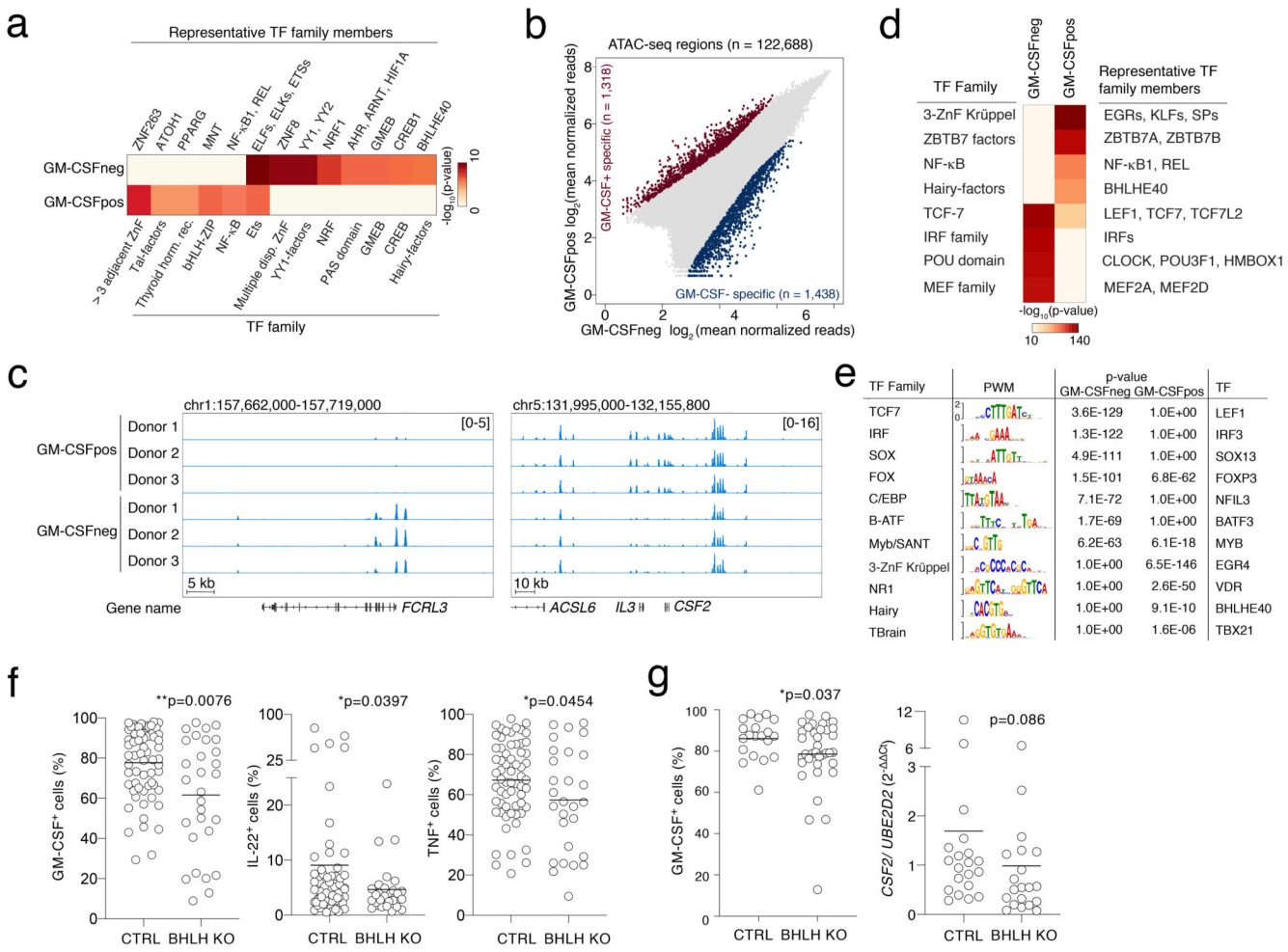

Figure 3. Identification of TFs regulating the inflammatory cytokine-producing phenotype.

a) PSCAN analysis on the promoter regions (-450 to +50 bp relative to the TSS) of genes identified as differentially expressed by RNA-seq in GM-CSF$^+$ or GM-CSF$^-$ cells. Selected factors are shown. The entire list of binding factors is provided in Suppl. Table 3. **b)** Scatterplot of ATAC-seq regions (n=3 independent donors). Blue and red dots indicate statistically significant accessible genomic regions (FDR < 0.01) that differ between GM-CSF$^+$ and GM-CSF$^-$ T cells, with absolute $\log_2$ FC ≥ 1, as determined by DiffBind using DESeq2. All other peaks are indicated as grey dots. **c)** Snapshots of ATAC-seq tracks for representative and relevant genes in the different donors. **d)** TF motif analysis in ATAC-seq regions specific of GM-CSF$^+$ and GM-CSF$^-$ T cells. **e)** TF binding site representation at accessible genomic sites identified by ATAC-seq in GM-CSF$^+$ and GM-CSF$^-$ T cells. Significance was determined by a two-tailed Welch's t-test using Pscan. The right column shows TFs that are also differentially expressed in GM-CSF$^+$ (SOX13, NFIL3, BATF3, VDR, BHLHE40, TBX21) and GM-CSF$^-$ cells (all other factors). **f)** Primary human memory T lymphocytes were transfected with ribonucleoparticles of Cas9 and gRNAs against exon 1/2 and exon 5 of *BHLHE40*. After single cell cloning and expansion, individual clones were tested for the presence of the deletion by PCR. Mean; Welch's or unpaired (TNF) t-test, two-tailed. Each dot represents one clone (n=at least 28). **g)** Same as

Europe PMC Funders Author Manuscripts
Europe PMC Funders Author Manuscripts

e) except that gRNAs against exon 1 and exon 2 of *BHLHE40* were used. N=36 clones from two independent human donors were selected for GM-CSF intracellular staining and *CSF2* expression. Mean; unpaired t-test with Welch's or Mann-Whitney correction, two-tailed. Each dot represents one clone.

Europe PMC Funders Author Manuscripts

Europe PMC Funders Author Manuscripts

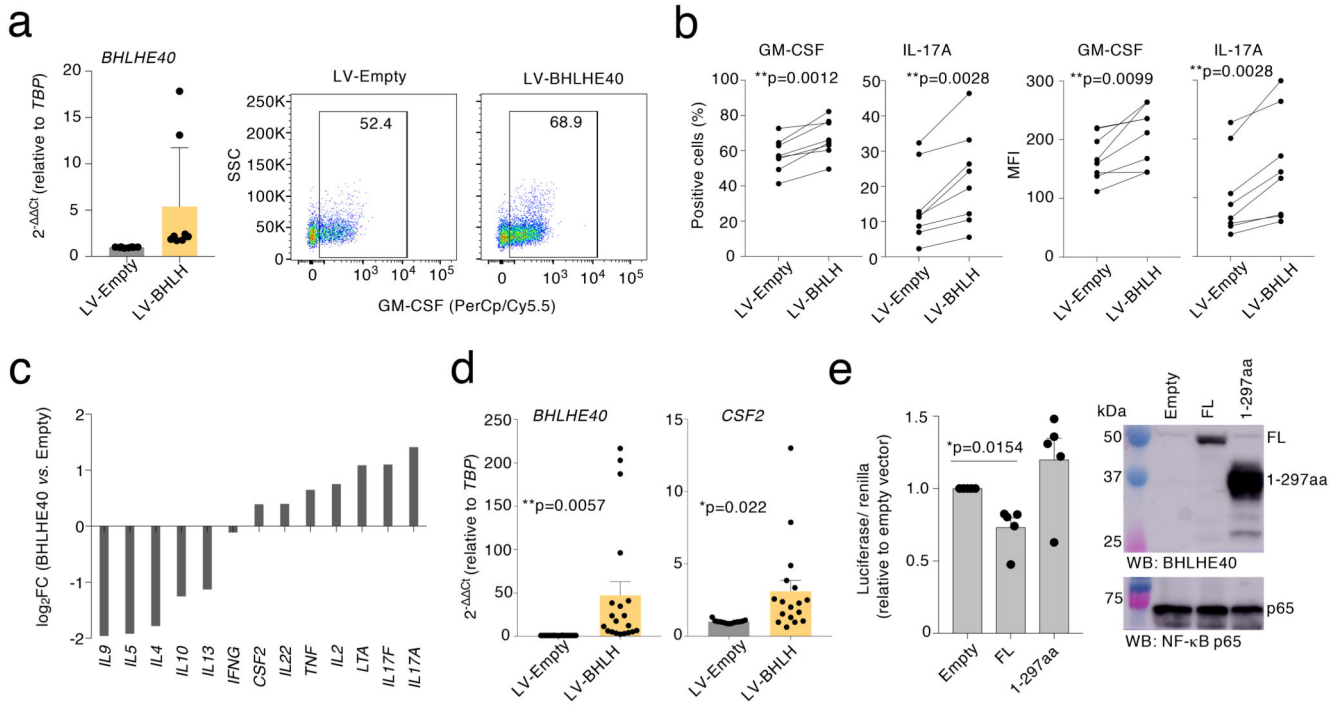

Figure 4. BHLHE40 affects inflammatory cytokine production in human memory T cells.

a) Freshly isolated memory T lymphocytes were activated with plate-bound anti-CD3 and anti-CD28 antibodies for 48 h prior to lentiviral transduction with either an empty vector or a BHLHE40 expression vector (LV-BHLH). Transduced cells were selected with puromycin, and further expanded for 10-12 days in the presence of IL-2. Expression of *BHLHE40* was measured by qRT-PCR (left, mean± SD) and GM-CSF production by intracellular staining (right). Each dot represents one individual experiment (n=8). The FACS plot on the right is representative of n=8 independent experiments. **b)** Percentage (left) and mean fluorescence intensity (MFI, right) of GM-CSF- and IL-17A-expressing cells in samples as in a). Each dot pair represents one individual human donor (n=8). Paired t-test, two-tailed. **c)** Memory $CD4^+$ T lymphocytes from three independent donors were transduced with either an empty lenti-vector or a BHLHE40 expression vector. After puromycin selection, cells were expanded in the presence of IL-2 for a few days, stimulated with PMA and ionomycin for three hours and gene expression analysis was performed with a Nanostring Sprint profiler. **d)** Jurkat T cells were transduced with lentiviral vectors and selected as in c), prior to measurement of *BHLHE40* and *CSF2* expression by qRT-PCR. Each dot represents one individual experiment (n=17). Mean ± SEM; unpaired t-test, two-tailed. **e)** HEK293 cells were transiently transfected with a luciferase reporter vector containing four consensus binding sites for BHLHE40. Cells were also co-transfected with either full-length (FL) human BHLHE40 or a truncated version (amino acids 1-297) lacking the C-terminal region. The graph on the left shows the results of n=5 independent experiments (mean ± SEM; paired t-test, two-tailed), while the immunoblot on the right shows expression of BHLHE40 in these samples (representative of n=at least 2 independent experiments).

Europe PMC Funders Author Manuscripts
Europe PMC Funders Author Manuscripts

Europe PMC Funders Author Manuscripts

Europe PMC Funders Author Manuscripts

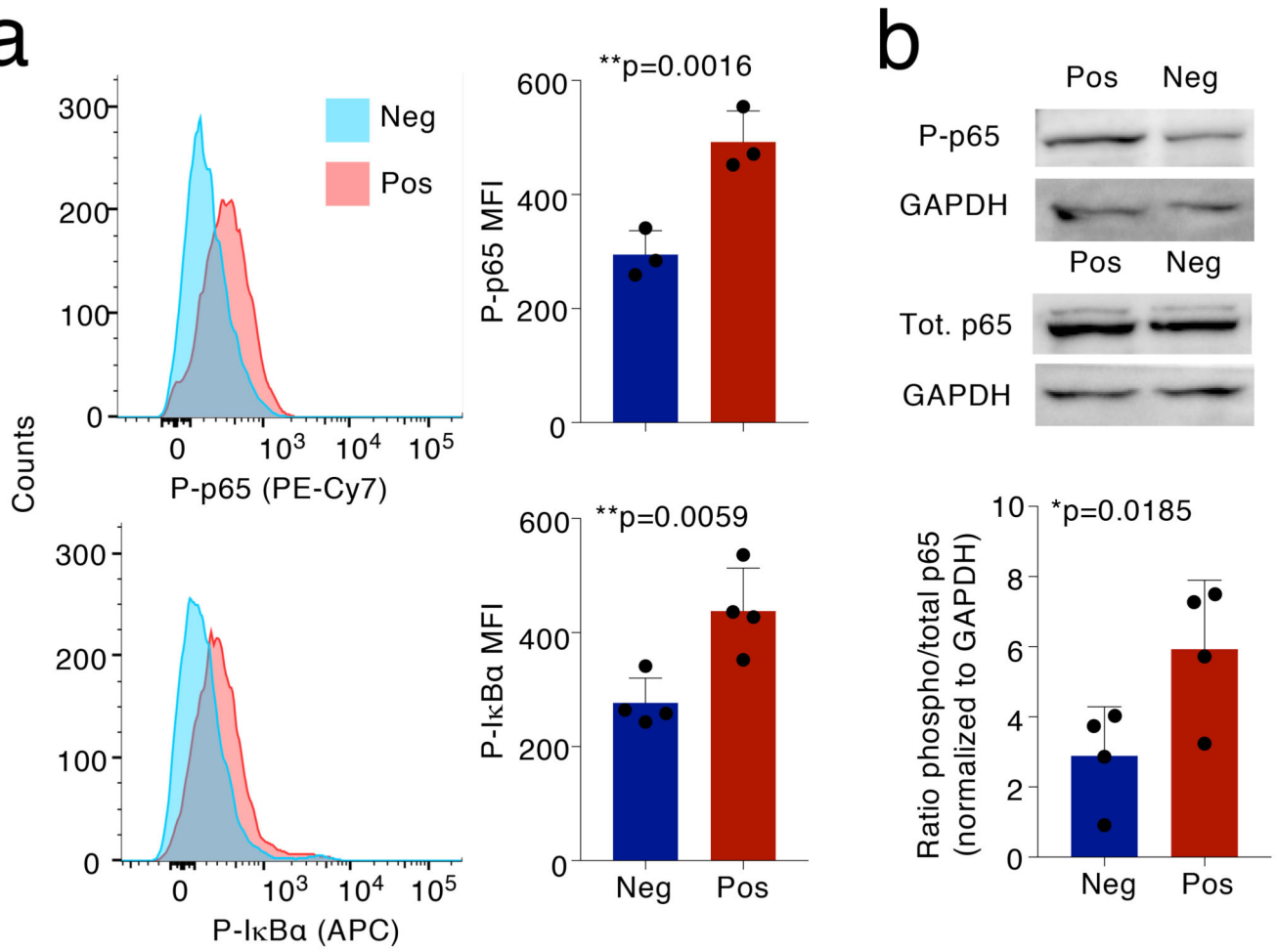

Figure 5. Phosphorylation of NF-κB p65 in GM-CSF$^+$ and GM-CSF$^-$ T cells.

a) T_{EM} cells were separated by GM-CSF secretion assay and sorting and left resting for 48h, followed by intracellular staining for phospho-p65 and phospho-IκBα. Left: one representative experiment; right: results of n=3 independent experiments. Each dot represents one donor (n=3). Mean ± SD; paired t-test, two-tailed. **b)** Cells were treated exactly as in a) except that phosphorylation of p65 was determined by immunoblot. Each dot represents one donor (n=4). Mean ± SD; paired t-test, two-tailed. The blot image is representative of n=4 independent experiments, quantified in the histogram below.

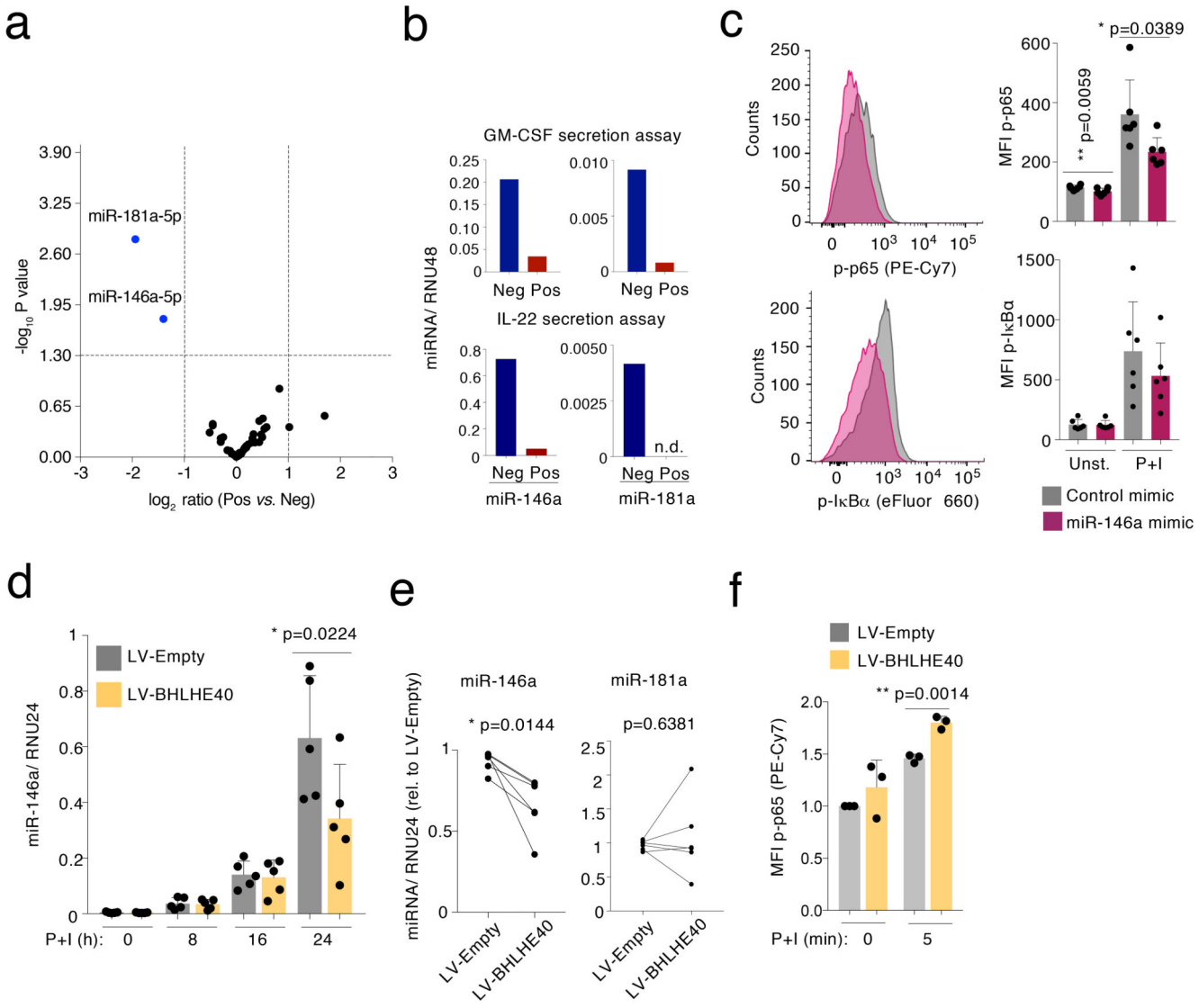

Figure 6. miR-146a expression is regulated by BHLHE40 and inhibits NF-κB p65 phosphorylation.

a) T_{EM} cells from n=6 independent donors were separated by GM-CSF secretion assay and FACS sorting, followed by RNA extraction and global miRNA analysis using Nanostring profiling (t-test, two-tailed). **b)** T_{EM} cells were separated by either GM-CSF (top) or IL-22 (bottom) secretion assays, and miRNA expression was measured by qRT-PCR. To obtain a sufficient number of cells for RNA extraction and qRT-PCR, n=3 donors were pooled after the GM-CSF secretion assays and n=8 independent donors were pooled after the IL-22 secretion assay. Technical replicates are not shown. n.d.: not detectable. **c)** Memory T lymphocytes were separated from peripheral blood and transiently transfected with miR-146a mimic or control oligonucleotides. After two days of culture, cells were stimulated for 5 min with PMA and ionomycin and phosphorylation of NF-κB p65 and IκBα was determined by intracellular staining (representative of n=6 experiments). Each dot represents one individual donor (n=6). Mean ± SD; paired t-test, two-tailed. **d)** Jurkat T cells

Europe PMC Funders Author Manuscripts
Europe PMC Funders Author Manuscripts

were stably transduced with a lentivirus to express BHLHE40. Cells were then stimulated with PMA and ionomycin for the indicated times prior to RNA extraction and measurement of miR-146a induction. Each dot represents one individual experiment (n=5). Mean ± SD; paired t-test, two-tailed. **e)** Primary memory T lymphocytes were transduced with a BHLHE40-expressing lentivirus. After selection and expansion of the transduced cells, expression of miR-146a and miR-181a was measured by qRT-PCR. Each dot pair represents one individual human donor (n=5). Paired t-test, two-tailed. **f)** Primary memory T lymphocytes were stably transduced with the indicated lentiviral vectors. After selection, cells were stimulated for 5 min with PMA and ionomycin, and NF-κB p65 phosphorylation was measured by intracellular staining. Mean ± SD; paired t-test, two-tailed; each dot represents one independent experiment (n=3).

Europe PMC Funders Author Manuscripts

Europe PMC Funders Author Manuscripts

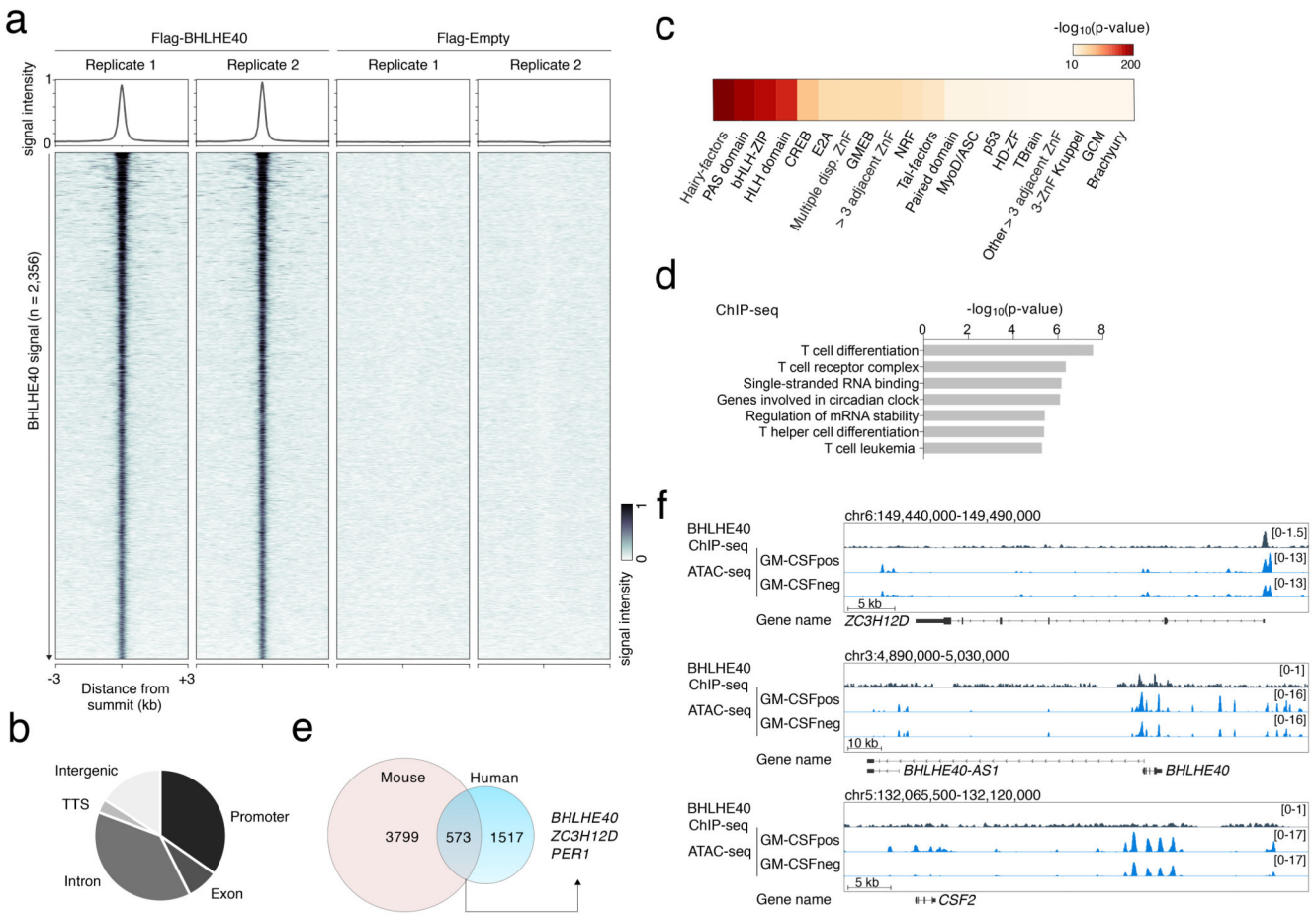

Figure 7. ChIP-seq of BHLHE40 identifies specific binding loci in the human genome.

a) Jurkat T cells were stably transduced to express Flag-tagged BHLHE40 or with a Flag empty vector. After crosslinking, chromatin was immunoprecipitated with an anti-Flag antibody and sequenced. Shown are the sequencing results of two independent transductions. Peak calling was performed independently for each biological replicate (n=2) using macs2 (FDR ≤ 0.05 and FE > 4), obtaining 2'356 consistent peaks showing an overlap of at least 50% of their length. **b)** Genomic distribution of the identified BHLHE40 ChIP-seq peaks in different genomic features. TTS: transcription termination site. **c)** Analysis of TF motifs enrichment. Local enrichment p-value with a two-tailed t distribution was calculated by PscanChIP using a window of 150bp centered on the summit of 2,356 peaks. **d)** GREAT analysis on the identified set of ChIP-seq peaks. The bar-plot show the -$\log_{10}$ of the p-values obtained by a binomial enrichment test. **e)** Overlap between our ChIP-seq dataset and the mouse Bhlhe40 ChIP-seq in T_H1 cells from Ref.[25]. **f)** Snapshots of ChIP-seq and ATAC-seq tracks for representative genes. *BHLHE40* transcription overlaps with an antisense transcript (*BHLHE40-AS1*).

Europe PMC Funders Author Manuscripts
Europe PMC Funders Author Manuscripts

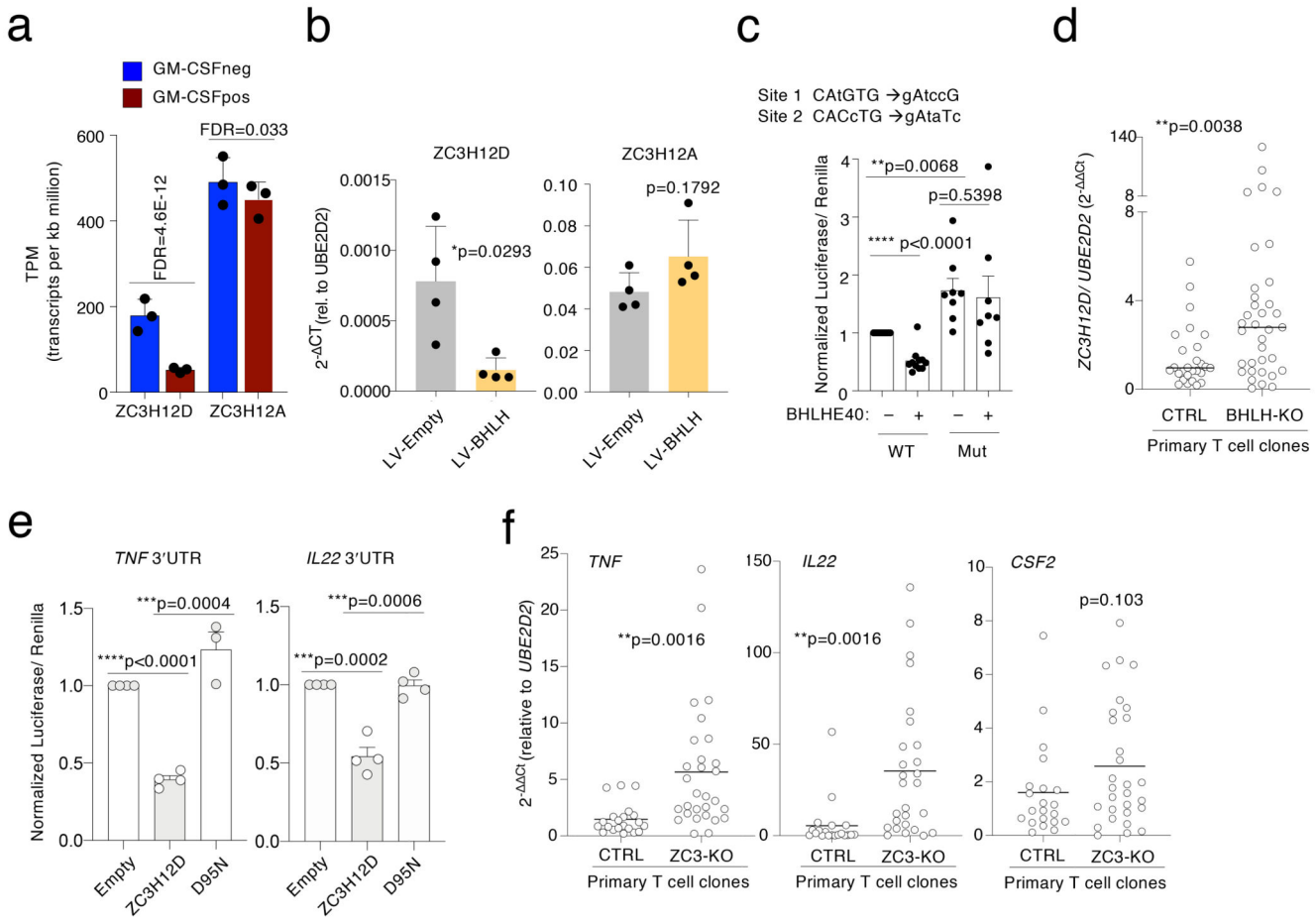

Figure 8. Direct regulation of ZC3H12D by BHLHE40 and effect on inflammatory cytokine expression in human T lymphocytes.

a) Expression of *ZC3H12D* and *ZC3H12A* in GM-CSF^{+} and GM-CSF^{-} T_{EM} cells, as determined by RNA-seq. Mean ± SD. **b)** Jurkat T cells were transduced to stably express BLHLE40, and expression of *ZC3H12D* and *ZC3H12A* was determined by qRT-PCR. Mean ± SD; paired t-test, two-tailed; each dot represents one independent experiment (n=4). **c)** The -285 to +349 region surrounding the *ZC3H12D* TSS was cloned in a luciferase reporter vector, with or without the indicated mutations in two BHLHE40 binding sites. Luciferase activity was determined upon co-transfection of HEK293 cells of the reporter vector with either a BHLHE40 expressing vector or an empty control. Mean ± SEM; paired t-test, two-tailed; each dot represents one independent experiment (n=8). **d)** Primary BHLHE40-KO clones (generated from 3 independent human donors) and controls were stimulated for 3h with PMA and ionomycin prior to RNA extraction and analysis of *ZC3H12D* expression by qRT-PCR. Median; each dot represents one clone (n=at least 26). Mann-Whitney test. **e)** The 3'UTR of the *TNF* and *IL22* genes was cloned downstream the luciferase gene in the pmirGLO vector. Luciferase activity was determined upon co-transfection of HEK293 cells of the reporter vector with a ZC3H12D expressing vector, either wild-type of mutated to abrogate RNase activity (D95N). Mean ± SEM; unpaired t-test, two-tailed; each dot represents one independent experiment (n=at least 3). **f)** Primary human memory T

Europe PMC Funders Author Manuscripts
Europe PMC Funders Author Manuscripts

lymphocytes (from two independent donors) were transfected with ribonucleoparticles of Cas9 and 2 gRNAs against *ZC3H12D*. After single cell cloning and expansion, individual clones were tested for the presence of indels in the *ZC3H12D* locus by mismatch cleavage assay. The clones were stimulated with PMA and ionomycin for 3 h prior to RNA extraction and analysis of cytokine mRNA expression by qRT-PCR. Mean; unpaired t-test, two-tailed. Each dot represents one clone (n=at least 21).

Europe PMC Funders Author Manuscripts

Europe PMC Funders Author Manuscripts